RSC Advances

PAPER

View Article Online
View Journal | View Issue

Cite this: *RSC Adv.*, 2025, **15**, 44649

Multifunctional N-substituted 2-pyridylbenzothiazole derivatives: singlet oxygen generation, protein binding, and photoactivated anticancer and antibacterial activities

Hanan A. Mohamed,[ab] Ayman A. Abdel-Shafi,[c] Hideyuki Miyatake,[d] Mohamed E. El-Khouly *[a] and Amr A. Nassrallah*[ef]

This study presents the optical characteristics, and biological characteristics of four N-substituted 2-pyridylbenzothiazole derivatives, namely 6-amino-5-(2-benzothiazolyl)-2-oxo-1-phenyl-1,2-dihydro-3-pyridinecarbonitrile (**BTZ-Ph**), 6-amino-5-(2-benzothiazolyl)-2-oxo-1-(4-chlorophenyl)-1,2-dihydro-3-pyridinecarbonitrile (**BTZ-ClPh**), 6-amino-5-(2-benzothiazolyl)-2-oxo-1-(4-methylphenyl)-1,2-dihydro-3-pyridinecarbonitrile (**BTZ-MePh**), and 6-amino-5-(2-benzothiazolyl)-2-oxo-1-(naphthalen-1-yl)-1,2-dihydro-3-pyridinecarbonitrile (**BTZ-Nap**). The steady-state absorption and emission properties of the examined compounds were assessed in acetonitrile solutions. The fluorescence quantum yields were determined to be 0.27 (**BTZ-Ph**), 0.24 (**BTZ-ClPh**), 0.28 (**BTZ-MePh**), and 0.25 (**BTZ-Nap**). The biological studies showed a significant interaction of the examined compounds with bovine serum albumin (BSA), where the binding constant (K), Stern–Volmer quenching constant (K_{sv}), and the number of binding sites were determined. Steady-state fluorescence and time-correlated single photon counting suggest a highly probable energy transfer pathway from the BSA singlet excited state to the examined compounds. The antibacterial activity was evaluated using disc diffusion and minimum inhibitory concentration (MIC) techniques under both dark and light conditions. The compounds exhibited significant antibacterial activity when subjected to blue illumination. The examined N-substituted 2-pyridylbenzothiazole derivatives exhibited markedly enhanced photo-cytotoxicity against human breast cancer MCF-7 (at IC_{50} values of 69.54, 49.78, 9.86, and 16.54 μg mL^{-1} for **BTZ-Ph**, **BTZ-ClPh**, **BTZ-MePh**, and **BTZ-Nap**, respectively) and human colorectal carcinoma HCT-116 cell lines (at IC_{50} values of 47.65, 147.98, 56.98, and 22.32 μg mL^{-1} for **BTZ-Ph**, **BTZ-ClPh**, **BTZ-MePh**, and **BTZ-Nap**, respectively) when subjected to blue light excitation at 450 nm. Molecular docking was employed to elucidate the interaction mechanism of the compounds with BSA, revealing that **BTZ-Ph** exhibited a higher binding energy. The determined BSA-binding constants correlated effectively with the antibacterial and cytotoxic outcomes, as well as the molecular docking data. Significantly, the compounds demonstrated encouraging singlet oxygen quantum yields in acetonitrile, ranging from 0.18 to 0.33 (detected *via* luminescence), suggesting their potential for cancer photodynamic therapy. These findings suggest the potential of these materials as a multifunctional platform for singlet oxygen generation, protein interaction, and photo-enhanced bioactivity.

Received 26th August 2025
Accepted 6th November 2025

DOI: 10.1039/d5ra06375b

rsc.li/rsc-advances

1. Introduction

Over the years, the investigation of novel pharmaceutical products has established the promising structure–activity correlation as a fruitful and rapidly advancing field of medicinal chemistry. To figure out active components across a broad spectrum of therapeutic domains within a restricted timeframe, the administration of compound derivatives facilitates the

[a]*Nanoscience Program, Faculty of Basic and Applied Sciences, Egypt-Japan University of Science and Technology (E-JUST), New Borg El-Arab City, Alexandria, Egypt. E-mail: mohamed.elkhouly@ejust.edu.eg*

[b]*Department of Chemistry, Faculty of Science, Kafrelsheikh University, Kafrelsheikh City, Egypt*

[c]*Department of Chemistry, Faculty of Science, Ain Shams University, 11566 Abbassia, Cairo, Egypt*

[d]*Nano Medical Engineering Laboratory, RIKEN, 2-1 Hirosawa, Wako-shi, Saitama, 351-0198, Japan*

[e]*Biotechnology Program, Faculty of Basic and Applied Sciences, Egypt-Japan University of Science and Technology (E-JUST), New Borg El-Arab City, Alexandria, Egypt. E-mail: amr.nassrallah@ejust.edu.eg*

[f]*Biochemistry Department, Faculty of Agriculture, Cairo University, Giza 12613, Egypt*

utilization of pharmaceuticals containing nitrogen and sulfur heterocycles, which are pivotal in numerous other developed fields, as well as in disciplines associated with specialized areas of pharmaceutical chemistry.[1] The heterocyclic substances have exhibited remarkable biological activity, and their research has been a fascinating area of medical chemistry for many years. A literature review shows that heterocyclic compounds and their derivatives with nitrogen and sulfur atoms offer special and adaptable scaffolds for the invention of new drugs.[2] Throughout, organic compounds involving pyridine and thiazole platforms have garnered sustained interest due to their diverse biological activities, including antiviral,[3] antifungal,[4] anticancer,[5] antimicrobial,[6] anti-hypertensive,[7] anti-inflammatory,[8] anti-histamine,[9] anticonvulsant,[10] and analgesic properties,[11] along with numerous other significant biological implications.

Bovine serum albumin (BSA) binds to heterocyclic compounds, such as pyridothiazole derivatives with nitrogen and sulfur atoms, through complex interactions mainly driven by hydrogen bonds, hydrophobic forces, and the structural bond with the BSA binding sites, which are primarily located around subdomains IIA and IIIA where important tryptophan residues assist in stabilizing the ligand through static quenching mechanisms.[12] The interactions described are essential for identifying drug delivery and pharmacokinetics, as BSA functions as a carrier protein with exceptional acceptor properties for several pharmaceutical components, serving as a dynamic resource in producing innovative drug candidates.[13–15] BSA is a crucial globular serum albumin utilized as a model protein in many investigations. The molecular weight of BSA is 66 000 Da and is composed of 582 amino acid residues. It includes 17 disulfide bridges and a free-SH group.[16–18] The structure consists of three unique homologous domains: I, II, and III. Each one of these domains is further subdivided into two subdomains, designated A and B. It includes two tryptophan residues, specifically Trp-213 and Trp-134. The Trp-134 is recognized to be situated in a hydrophilic environment near the protein surface (sub-domain-I B). Trp-213 is positioned within the largest hydrophobic cavity, specifically in domain II (subdomain-II A). The primary binding regions of BSA are located within subdomains IIA and IIIA.[19–22] The interactions that occur between BSA and compounds provide significant insights into the drug's intake and distribution. The UV-visible absorbance and fluorescence emission of amino acid residues in BSA are significant in protein–ligand interactions because of their high specificity, exceptional sensitivity, and immediate reaction capabilities. Additionally, UV-visible absorbance, fluorescence emission, and lifetime studies offer critical insights into the binding mechanism, binding method, binding constants, and location.[23–27]

Photodynamic therapy (PDT) is a low-invasive, targeted therapeutic approach that employs a photosensitizer (a light-sensitive medicine), a particular wavelength of illumination, and oxygen to generate reactive oxygen species (ROS) that eradicate targeted cells. The photosensitizer absorbs light, becomes energized, and transfers energy to oxygen molecules, producing reactive oxygen species (ROS) that trigger cellular death. Photodynamic therapy (PDT) has demonstrated considerable utility in microbial (antimicrobial PDT) and oncological treatments, garnering increasing medical and academic attention.[28] The photosensitizer (PS) must produce reactive oxygen species (ROS) when exposed to light and oxygen, and it should exhibit a significant amount of excited electronic triplet states and singlet oxygen.[29] Singlet oxygen ($^1O_2$), the lowest excited state of the dioxygen molecule, could be produced using photochemical and chemical methods. The predominant photochemical process includes energy transfer from a triplet excited photosensitizer ($^3PS^*$) to nearby molecular oxygen.[30–32] The features of the photosensitizer significantly influence the efficiency of PDT, and heterocyclic compounds, particularly those incorporating nitrogen and sulfur atoms, are emerging as potential options owing to their adjustable photophysical and biological properties.[33] Heterocyclic molecules bearing N and S atoms, including pyridothiazole derivatives, have attracted considerable attention as effective photosensitizers in photodynamic therapy (PDT) against cancer and bacterial infections. When these compounds are exposed to light, they produce reactive oxygen species that damage important parts of the cells, leading to their death. Among these, phenothiazinium dyes such as *methylene blue* and *toluidine blue O* are widely used for antimicrobial PDT, showing potent bactericidal effects against Gram-positive and Gram-negative bacteria under red-light exposure.[34] Similarly, benzophenothiazinium derivatives like *EtNBS* demonstrate significant phototoxicity toward cancer cells and are effective even under hypoxic conditions.[35] Recent studies have also highlighted thionated heterocycles, such as thieno[3,4-*d*]pyrimidin-4(3*H*)-thione (ThiathioHX), as promising non-porphyrinic PDT agents with oxygen-independent activity in tumor environments.[36]

Motivated by the interesting photophysical and biological properties of pyridine and benzothiazole substitutes, we examined four new N-substituted 2-pyridylbenzothiazole derivatives to investigate their biomedical activities. These compounds are: 6-amino-5-(2-benzothiazolyl)-2-oxo-1-phenyl-1,2-dihydro-3-pyridinecarbonitrile (**BTZ-Ph**), 6-amino-5-(2-benzothiazolyl)-2-oxo-1-(4-chlorophenyl)-1,2-dihydro-3-pyridinecarbonitrile (**BTZ-ClPh**), 6-amino-5-(2-benzothiazolyl)-2-oxo-1-(4-methylphenyl)-1,2-dihydro-3-pyridinecarbonitrile (**BTZ-MePh**), and 6-amino-5-(2-benzothiazolyl)-2-oxo-1-

Mohamed E. El-Khouly, an Egyptian-born chemist, earned his PhD in chemistry from Tohoku University, Japan, in 2002. He conducted postdoctoral research in Japan with funding from Venture Business Laboratory (Chiba University, 2003–2004), Center of Excellence (Tohoku University, 2004–2006), and the Japan Society for the Promotion of Science (Tohoku University, 2006–2008). From 2008 to 2012, he served as a specially appointed Associate Professor at the Department of Materials and Life Science, Graduate School of Engineering, Osaka University. Dr El-Khouly's research primarily focuses on artificial photosynthesis, supramolecular light harvesitng complexes, solar fuels, environmental chemsitry, and biomedical applications.

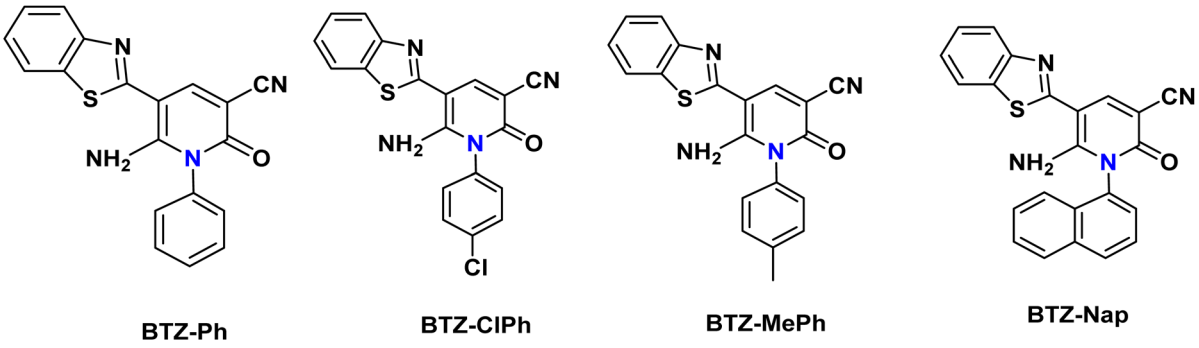

Fig. 1 Structures of the studied N-substituted 2-pyridylbenzothiazole derivatives.

(naphthalen-1-yl)-1,2-dihydro-3-pyridinecarbonitrile (**BTZ-Nap**) (Fig. 1). This study focuses on their photophysical properties, their interaction with bovine serum albumin (BSA), and their potential as photosensitizers for photodynamic therapy (PDT) against cancer and bacterial infections.

2. Experimental

2.1. Synthesis of the four N-substituted 2-pyridylbenzothiazole derivatives

The pyridine-benzothiazole chemical group under investigation was synthesized through the reaction of 2-(benzo[*d*]thiazol-2-yl)-3-(dimethylamino)acrylonitrile (10 mmol) with *N*-aryl-2-cyanoacetamides (10 mmol) and potassium hydroxide in dry 1,4-dioxane (30 mL) under reflux at 101 °C for 1 h, then cooled and poured onto iced water; the resulting precipitate was filtered off and recrystallized from ethanol. The reaction yield of the four compounds was around 80% and they were characterized by FT-IR and HNMR (Fig. S1 and S2) according to established literature, Scheme 1.[37]

2.2. Instruments and measurements

The optical absorption spectra of the four N-substituted 2-pyridylbenzothiazole derivatives were recorded using a UV-2600 spectrophotometer (Shimadzu, Japan) equipped with 1 cm quartz cuvettes at room temperature. To evaluate the interaction between BSA and the compounds, absorption titration experiments were performed by recording the absorption spectra of BSA solutions in the absence and presence of the four N-substituted 2-pyridylbenzothiazole derivatives. Stock solutions of the thiazole derivatives were gradually added to 2.0 mL of BSA solution (18 μM), and the corresponding changes in the BSA absorption spectra were determined after each addition.

The fluorescence measurements were examined the four N-substituted 2-pyridylbenzothiazole derivatives were recorded using utilizing RF6000 spectrofluorometer (Shimadzu, Japan). The fluorescence quenching experiment employed a fixed concentration of BSA solution (18 μM) while incrementally adding varying amounts of four N-substituted 2-pyridylbenzothiazoles. The fluorescence spectra were obtained at an excitation wavelength of 278 nm, with emission measured between 300 and 600 nm following each quencher addition, and the findings were then evaluated.

The fluorescence quantum yields (Φ_f) of the examined compounds were calculated utilizing coumarin 460 as a reference ($\Phi_{ref} = 0.73$ in ethanol)[38,39] according to eqn (1).

$$\Phi_s = \Phi_r \times \frac{F_s}{F_r} \times \frac{A_r}{A_s} \quad (1)$$

Φ_s and Φ_r denote the sample's and reference's quantum yields, respectively. F_s and F_r represent the integrated values of the sample and reference emission spectra, respectively. A_r and A_s refer to the optical density of the reference and sample, respectively, measured at 370 nm.

Fluorescence lifetimes were measured utilizing the Time-Correlated Single Photon Counting (TCSPC) apparatus (HORIBA Scientific), employing NanoLED pulsed diode light source (at 280 nm) as the excitation wavelength and 340 nm as the emission wavelength. Upon excitation, the fluorescence decay profiles of BSA (18 μM) were measured both in the absence and presence of the examined compounds and were analyzed with the 64-decay analysis software to estimate the fluorescent lifetimes.[40]

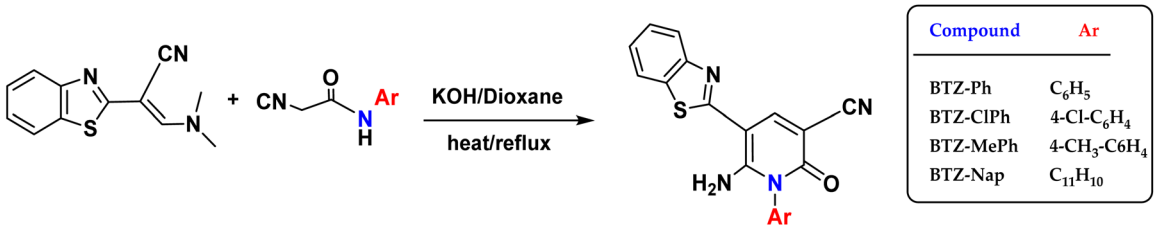

Compound	Ar
BTZ-Ph	C_6H_5
BTZ-ClPh	4-Cl-C_6H_4
BTZ-MePh	4-CH_3-C6H_4
BTZ-Nap	$C_{11}H_{10}$

Scheme 1 A schematic diagram of the synthesis of four N-substituted 2-pyridylbenzothiazole derivatives.

Singlet oxygen quantum yields (Φ_Δ) are detected directly by measurement of singlet oxygen luminescence emission at 1272 nm following photoexcitation of the examined compounds at ambient temperature in acetonitrile and compared it with the reference $[Ru(bpy)_3]^{2+}$ at zero time in acetonitrile solution.[41] The compounds are excited using the third harmonic of a Q-S Nd:YAG laser (λ = 355 nm, ~8 ns pulse length, pulse energy ≤20 mJ) incorporated with LP980 from Edinburgh instruments laser flash photolysis system in emission mode. The luminescent signal of singlet oxygen ($^1O_2$) at a wavelength of 1275 nm was measured using the Hamamatsu H10330-45 near-infrared (NIR) detector. The optical densities of the substance under study and the standard were equated at a wavelength of 355 nm.

2.3. Antibacterial activity

The antibacterial activity of the benzothiazolyl-pyridinecarbonitrile derivatives was evaluated against three pathogenic bacterial strains: *Salmonella enterica* (ATCC 14028), *Staphylococcus aureus* (ATCC 25923), and *Escherichia coli* (ATCC 25922). Stock solutions of each compound were prepared in dimethyl sulfoxide (DMSO) and diluted with sterile double-distilled water to obtain final concentrations of 25 μg mL^{-1} and 50 μg mL^{-1}.

Bacterial cultures were grown overnight in Luria–Bertani (LB) medium at 37 °C, and cell suspensions were adjusted to a 0.5 McFarland standard (≈1.5 × 10^8 CFU mL^{-1}). For photodynamic treatment, samples were irradiated for 20 min at 5.2 mW cm^{-2} (dose ≈ 6.24 J cm^{-2}) using a blue LED light source (440–490 nm) at a fixed distance of 5 cm, while corresponding control samples were maintained in the dark.[42]

2.3.1. Disc. diffusion assay. LB agar plates were inoculated by uniformly swabbing with bacterial suspensions. Sterile paper discs (5 mm diameter) were impregnated with 10 μL of each compound solution (25 or 50 μg per mL per disc.) and placed on the agar surface. Plates were divided into two groups: one irradiated with blue light and the other incubated in the dark. After 24 h incubation at 37 °C, the inhibition zones were measured in millimeters. DMSO-treated discs served as negative controls.

2.3.2. MIC determination. Minimum inhibitory concentrations (MICs) were determined using the broth microdilution method in 24-well microtiter plates. Serial two-fold dilutions of each compound were prepared in LB medium, and wells were inoculated with ≈5 × 10^5 CFU mL^{-1} bacterial suspensions. As in the disc diffusion assay, plates were divided into light-irradiated and dark-incubated groups. After 24 h incubation at 37 °C, the MIC was defined as the lowest concentration with no visible bacterial growth.[43] All experiments were conducted in triplicate, and results are reported as mean ± standard deviation. Statistical analysis was performed using one-way ANOVA, with $p < 0.05$ considered statistically significant.

2.4. *In vitro* cytotoxic activity

The anticancer potential of the benzothiazolyl-pyridinecarbonitrile derivatives was evaluated against two human cancer cell lines—MCF-7 (breast adenocarcinoma, ATCC® HTB-22™) and HCT-116 (colorectal carcinoma, ATCC® CCL-247™)—along with BJ-1 normal human skin fibroblasts (ATCC® CRL-2522™) as a non-cancerous control.

Stock solutions (10 mg mL^{-1}) of each compound were prepared in dimethyl sulfoxide (DMSO) and diluted in culture medium to final working concentrations of 0.5, 1, 5, 10, 50, and 100 μg mL^{-1} immediately before treatment. Experiments were performed under two conditions: in the dark and following blue light irradiation.

Cell lines were cultured in Dulbecco's Modified Eagle Medium (DMEM) supplemented with 10% fetal bovine serum (FBS), 1% penicillin–streptomycin, and 1% L-glutamine, and maintained at 37 °C in a humidified incubator with 5% CO_2. Cells were seeded in 24-well plates at a density of 5 × 10^6 cells per well and allowed to adhere for 24 h before compound exposure. For the light-treated groups, cells were incubated with test compounds for 6 h, then irradiated with a blue LED source (440–490 nm, 5.2 mW cm^{-2} (dose ≈ 6.24 J cm^{-2})) for 20 min at a fixed distance of 5 cm. Dark control groups were completely shielded from light. After treatment, cells were incubated for an additional 24 h at 37 °C.

Cell viability was assessed by the MTT assay.[46] Briefly, 20 μL of MTT solution (5 mg mL^{-1} in PBS) was added to each well and incubated for 4 h. The resulting formazan crystals were dissolved in 100 μL of DMSO, and absorbance was measured at 570 nm using a microplate reader. Cell viability was expressed as a percentage relative to untreated controls.[44]

All experiments were conducted in triplicate, and results are presented as mean ± standard deviation. IC_{50} values (compound concentration causing 50% reduction in viability) were calculated using nonlinear regression analysis. Statistical comparisons between light-treated and dark groups were performed using one-way ANOVA followed by Tukey's *post hoc* test, with $p < 0.05$ considered statistically significant.

2.5. Computational molecular docking studies

Molecular docking investigations were conducted to identify the binding sites and modes of the developed compounds on bovine serum albumin (BSA), distinguished by its several binding pockets. The simulations employed the crystal structure of BSA complexed with 3,5-diiodosalicylic acid (PDB ID: 4jk4).[45] All computations were performed utilizing ICM-Pro software.[46] Two separate methodologies were used to determine the most potential binding locations. Initially, docking was directed towards three established ligand binding sites on BSA: Drug Site 1 (**DS1**), Drug Site 2 (**DS2**), and Drug Site 3 (**DS3**), the latter occupying the top region of the FA1 fatty acid pocket.[45] Docking for these targeted simulations was conducted employing the co-crystallized ligand, 3,5-diiodosalicylic acid, as a template. Simultaneously, non-template docking experiments were performed for the same sites to facilitate unbiased pose prediction. A comprehensive search for all possible binding pockets on the BSA surface was carried out with the icmPocketFinder algorithm.[47] Pockets exhibiting a Drug-Like Density (DLID) score exceeding 0.6 were identified as promising binding sites for subsequent docking simulations. The DLID score is an

indicator that quantifies the "druggability" of a binding site, with values exceeding 0.5 often regarded as druggable. All simulations employed the 4D SCARE (Scanning and Refinement) docking protocol.[48] This method explicitly considers the adaptability of receptor sidechains within the binding pocket during ligand localization and optimization, therefore offering a more accurate representation of the binding interaction.

3. Results and discussion

3.1. Optical properties and lifetime of the N-substituted 2-pyridylbenzothiazole derivatives

The UV-vis absorption and emission spectra of the benzothiazolyl-pyridinecarbonitrile derivatives in acetonitrile were obtained to elucidate their optical properties. Fig. 2a of the UV-vis analysis demonstrates that the absorption spectra of all examined substances display a prominent absorption band at 372 nm, accompanied by two weaker absorption bands at 329 nm and 476 nm. The absorption bands at 326 and 379 nm could originate from π–π* transitions, whereas the absorption band at the longer wavelength of 476 nm comes from the n–π* transition. The fluorescence characteristics of the investigated compounds in acetonitrile displayed prominent emission bands in the 410–424 nm region when the samples received an excitation of 372 nm (Fig. 2b). Based on earlier studies, the fluorescence quantum yields of the synthesized compounds in ethanol determined to be 0.28, 0.24, 0.27, and 0.25 for compounds **BTZ-Ph**, **BTZ-ClPh**, **BTZ-MePh**, and **BTZ-Nap**, respectively.[37] These optical absorption and emission features agree well with the literature.[37] Furthermore, compounds **BTZ-Ph**, **BTZ-ClPh**, **BTZ-MePh**, and **BTZ-Nap** demonstrated mono-exponentially fluorescence decay curves (Fig. 2c), with lifetimes recorded at 0.81, 0.59, 1.18, and 0.84 ns, respectively. The fluorescence lifetimes are within the ideal range for facilitating intersystem crossing (ISC) to the triplet excited state, promoting singlet oxygen generation ($^1O_2$).[49]

3.2. BSA binding studies

3.2.1. UV spectral studies. Finding the complex formation between serum albumin and bioactive compounds can be done easily and effectively with UV absorption spectroscopy.[50] Fig. 3 displays the absorbance spectra of BSA with increasing concentrations of **BTZ-Ph**, **BTZ-ClPh**, **BTZ-MePh**, and **BTZ-Nap**. The characteristic BSA peak at 278 nm, due to π–π* transitions of Trp, Tyr, and Phe residues,[51] showed a concentration-dependent increase in absorbance and a minor redshift (1–2 nm) upon derivative addition. These changes confirm the formation of an N-substituted 2-pyridylbenzothiazole-BSA complex and suggest conformational changes in BSA.[52] The

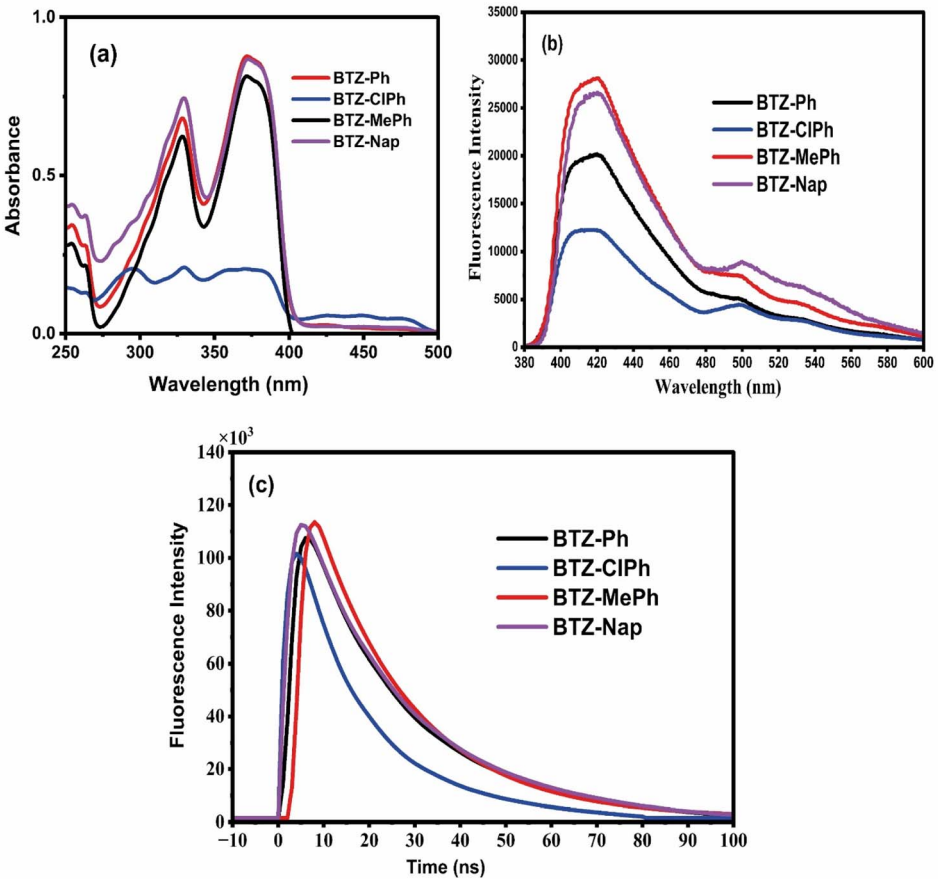

Fig. 2 Absorption (a) and emission (b) spectra of the indicated compounds in acetonitrile; λ_{ex} = 372 nm. (c) Fluorescence lifetime decay profiles in acetonitrile; λ_{ex} = 372 nm.

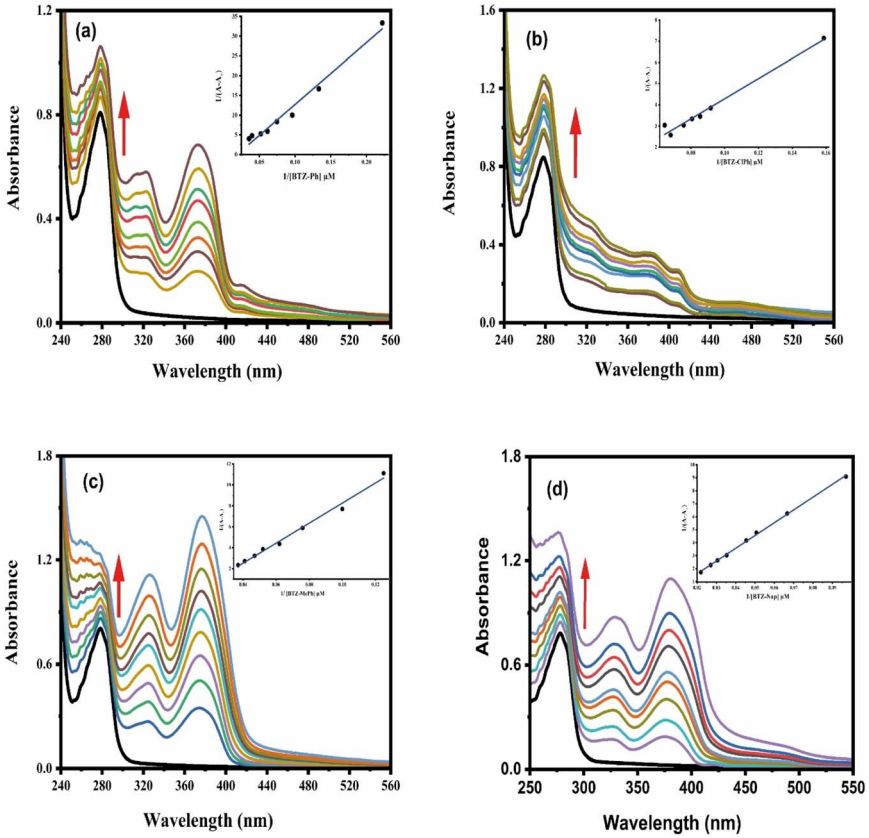

Fig. 3 Variations in BSA's UV-vis absorption spectra (18 μM). At 278 nm upon the addition of various concentrations of (a) **BTZ-Ph**, (b) **BTZ-ClPh**, (c) **BTZ-MePh**, and (d) **BTZ-Nap**. Stern–Volmer graphs are insets.

absorption peak at in Bovine Serum Albumin (BSA), attributed to the transition of aromatic amino acid residues (Tyr, Trp, Phe), correlates with the polarity of their microenvironment. The presence of additional aromatic residues from the ligands (**BTZ-Ph**, **BTZ-ClPh**, **BTZ-MePh**, and **BTZ-Nap**) increases the absorption intensity. The overall binding affinity, measured by (Table 1) and eqn (2), follows the order: (i) **BTZ-ClPh** exhibits the highest affinity due to the chlorine substituent, which enhances binding through both hydrophobic contacts and halogen bonding.[53] (ii) **BTZ-MePh** shows moderate binding; its methyl group increases hydrophobicity but lacks strong directional interactions.[54] (iii) **BTZ-Nap** offers extended stacking but is hindered by steric effects. (iv) **BTZ-Ph** shows the weakest binding due to the absence of substituents to promote stronger interactions.

$$\frac{1}{A_{obs} - A_0} = \frac{1}{A_c - A_0} + \frac{1}{K_b A_c - A_0[\text{compound}]} \quad (2)$$

The spontaneity of the drug–BSA binding for **BTZ-Ph**, **BTZ-ClPh**, **BTZ-MePh**, and **BTZ-Nap** is indicated by their negative change in Gibbs free energy ($\Delta G°$). Calculated using eqn (3), the values are −5.18, −5.80, −5.45, and −5.39 kcal M^{-1}, respectively. These negative values confirm the spontaneous formation of all compound-BSA complexes.[55]

$$\Delta G° = -RT \ln K_b \quad (3)$$

3.2.2. Steady state emission and fluorescence lifetime measurements. Bovine Serum Albumin (BSA) exhibits intrinsic fluorescence primarily from its tryptophan and tyrosine residues, with tryptophan having the highest intensity.[56] Tryptophan's fluorescence is highly sensitive to its microenvironment, making it an excellent endogenous fluorescent biomarker for studying BSA's interactions with bioactive molecules.[57] Fluorescence quenching of BSA results from various molecular interactions, such as complex formation and energy transfer.[58–61] Synchronous fluorescence spectroscopy is a sensitive and effective technique, offering increased simplicity and reduced spectral bandwidth, used to probe the microenvironment and conformational changes of these amino acid residues.[62]

The binding affinity of the four N-substituted 2-pyridylbenzothiazoles for BSA was determined by examining their influence on BSA's fluorescence. As illustrated in Fig. 4, all four compounds caused a substantial quenching of the BSA emission band at 339 nm. The decrease in initial fluorescence intensity was 76.7%, 84.1%, 84.5%, and 80.4% for **BTZ-Ph**, **BTZ-ClPh**, **BTZ-MePh**, and **BTZ-Nap**, respectively. Subsequent analysis using the inset Stern–Volmer plots and eqn (S1)[63] yielded

Table 1 Binding constants of BSA with N-substituted 2-pyridylbenzothiazole derivatives

Compounds	K_b (10^4 M^{-1})	ΔG (kcal M^{-1})	N	K_q (10^{13} M^{-1} s^{-1})	K_{SV} (10^5 M^{-1})	f_a
BTZ-Ph	0.64	−5.18	1.32	2.08	1.19	0.9 ± 0.3
BTZ-ClPh	1.80	−5.80	1.70	6.89	3.93	0.97 ± 0.4
BTZ-MePh	1.00	−5.45	1.08	2.45	1.40	0.99 ± 0.01
BTZ-Nap	0.90	−5.39	1.18	1.78	1.02	0.95 ± 0.2

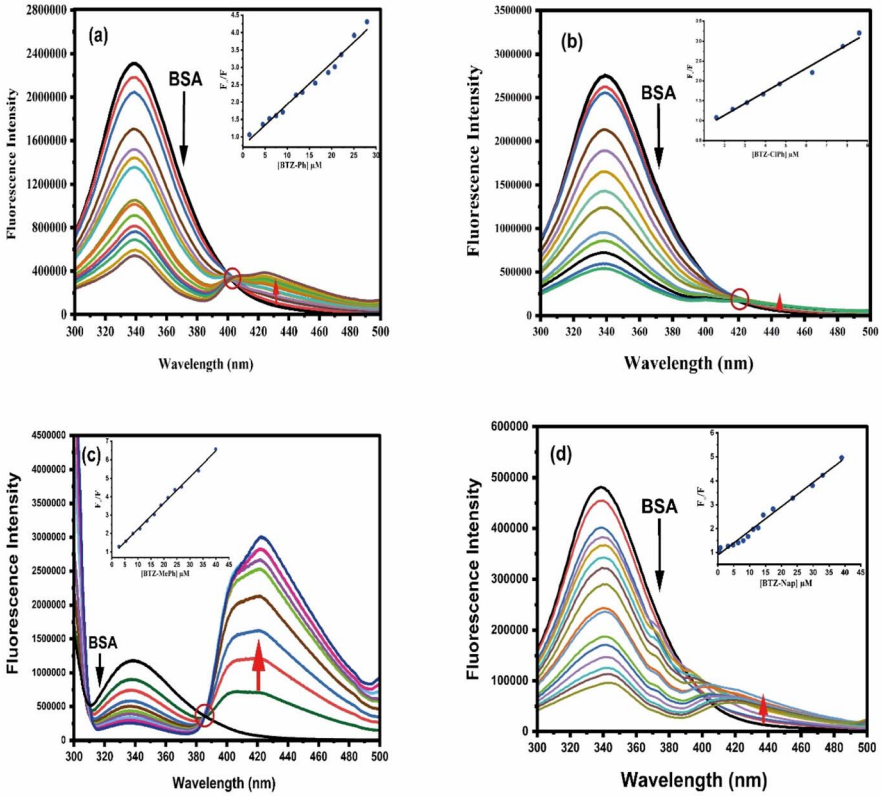

Fig. 4 Fluorescence quenching of BSA induced by different concentrations of (a) **BTZ-Ph** (0–28 μM), (b) **BTZ-ClPh** (0–12 μM), (c) **BTZ-MePh** (0–27 μM), and (d) **BTZ-Nap** (0–13 μM). (Inset) Stern–Volmer plots.

the following values: **BTZ-Ph** (1.4 $\times 10^5$ M^{-1}), **BTZ-ClPh** (1.19 $\times 10^5$ M^{-1}), **BTZ-MePh** (3.93 $\times 10^5$ M^{-1}), and **BTZ-Nap** (1.02 $\times 10^5$ M^{-1}). Furthermore, the values of n (the number of binding sites), and fa (the fraction of the initial fluorescence of BSA that is accessible to the N-substituted 2-pyridylbenzothiazole) were determined using Fig. S3, S4, eqn (S1) and (S4), while the quenching rate constant k_q was calculated by eqn (S3) (Table 1).

As seen from Fig. 4, the emission intensity of BSA was significantly quenched accompanied by formation of the singlet states of the examined four N-substituted 2-pyridylbenzothiazoles derivatives. This suggests the efficient quenching of the singlet state of BSA (3.76 eV) through the energy transfer process to populate the singlet state of the examined N-substituted 2-pyridylbenzothiazole derivatives (~2.88 eV). The strong overlap between the emission spectrum of BSA and absorption spectra of N-substituted 2-pyridylbenzothiazole derivatives provide further evidence about the occurrence of Förster resonance energy transfer (FRET).[64]

From Fig. 4, it's clear the emission intensity of BSA significantly quenched as the four examined N-substituted 2-pyridylbenzothiazoles derivatives formed singlet states. This suggests efficient singlet-state quenching of BSA (3.76 eV) occurred *via* energy transfer to populate the singlet state of the examined pyridylbenzothiazole derivatives (~2.88 eV). Further evidence for Förster resonance energy transfer (FRET) is provided by the strong overlap between the BSA emission spectrum and the absorption spectra of the N-substituted 2-pyridylbenzothiazole derivatives (Fig. S5).

Table 2 The efficacy of energy transfer, the overlap integral, and the distance parameters of **BTZ-Ph**, **BTZ-MePh**, and **BTZ-Nap**

Compound	J (10^{-16} L mol^{-1} cm^3)	R_0 (nm)	r (nm)	E (%)
BTZ-Ph	1.17	1.22	1.26	0.45
BTZ-ClPh	1.71	1.30	1.45	0.34
BTZ-MePh	1.23	1.23	1.28	0.44
BTZ-Nap	1.56	1.28	1.40	0.36

As is known, the rates of FRET theory depend on the distance between the donor and acceptor, the orientation of their dipoles, and the extent of overlap between the donor's emission spectrum and the acceptor's absorption spectrum. The energy transfer efficiency (E) can be assessed by the distance (r) between the donor (BSA) and the examined N-substituted 2-pyridylbenzothiazole derivatives in the protein using eqn (4).

$$E = 1 - \frac{F}{F_0} = R_0{}^6 / \left(R_0{}^6 + r^6\right) \quad (4)$$

where F and F_0 represent the fluorescence intensity of BSA in the presence and absence of the acceptor, respectively; r denotes the distance between the acceptor and donor; R_0 signifies the critical distance for 50% energy transfer, which may be computed using eqn (5).

$$R_0{}^6 = 8.8 \times 10^{-25}\, K^2 N^{-4} \Phi J \quad (5)$$

In the present situation, the spatial orientation factor of the dipole is $K^2 = 2/3$, the medium (water) refractive index is $N = 1.333$, and the fluorescence quantum yield of the donor BSA is $\Phi = 0.15$.[65] The spectral overlap integral (J), derived from the overlap of the acceptor UV absorption and donor fluorescence emission spectra, is expressed using eqn (6).

$$J = \frac{\sum F(\lambda)\varepsilon(\lambda)\lambda^4 \Delta\lambda}{\sum F(\lambda)\Delta\lambda} \quad (6)$$

Here, $F(\lambda)$ denotes the fluorescence intensity of BSA at wavelength λ, while $\varepsilon(\lambda)$ signifies the molar absorption coefficient of the examined compounds (**BTZ-Ph**, **BTZ-ClPh**, **BTZ-MePh**, and **BTZ-Nap**) at wavelength λ. The intersection of the BSA emission spectra with the absorption spectra of **BTZ-Ph**, **BTZ-ClPh**, **BTZ-MePh**, and **BTZ-Nap** is illustrated in Fig. S3, while the recorded values of J, r, R_0, and E are presented in Table 2. The r values for all examined pyridothiazoles are below 8 nm, indicating a significant possibility of non-radiative energy transfer process.[66] The efficiency of the energy transfer processes was determined to be 0.45, 0.44, 0.36, and 0.34 for BSA/**BTZ-Ph**, BSA/**BTZ-ClPh**, BSA/**BTZ-MePh**, and BSA/**BTZ-NaP**, respectively.

The time-resolved fluorescence spectral features of the BSA/N-substituted 2-pyridylbenzothiazoles interaction confirmed the steady-state emission measurements. Upon excitation at 280 nm, the fluorescence decay profile of the unbound BSA single state, monitored at 340 nm exhibited a mono-exponential decay with a fluorescence lifetime of 5.70 ns (Fig. 5). In contrast, the interaction with N-substituted 2-pyridylbenzothiazoles

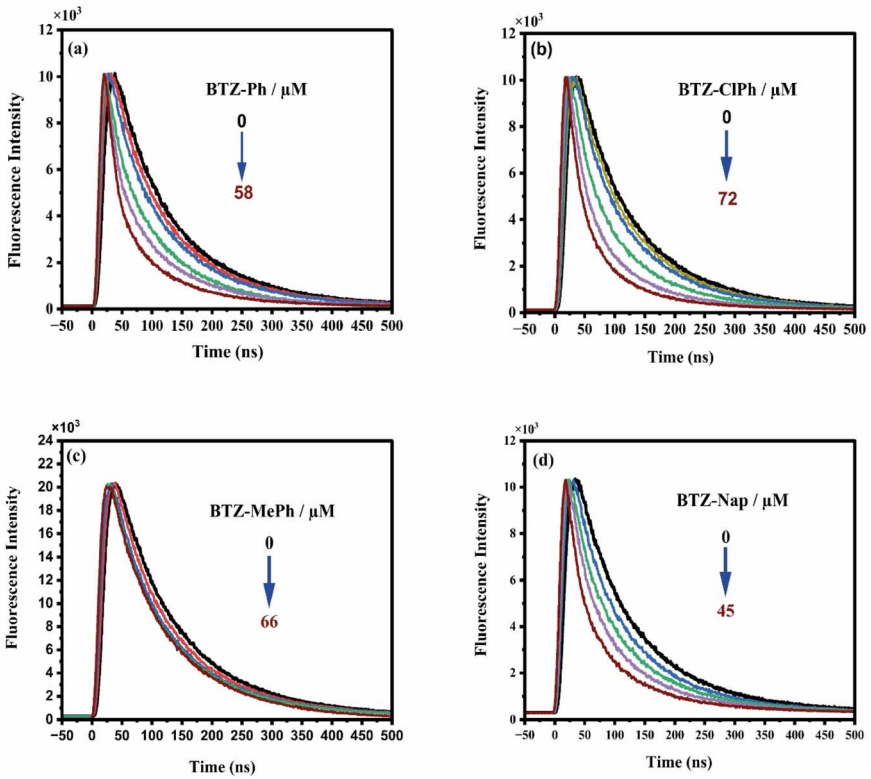

Fig. 5 Fluorescence lifetime decay profiles of BSA (18 μM) in the absence and presence of **BTZ-Ph** (a), **BTZ-ClPh** (b), **BTZ-MePh** (c), and **BTZ-Nap** (d).

caused significant quenching of the BSA singlet-state fluorescence lifetime. The observed short lifetime component for the complex confirms that dynamic quenching occurred through Förster resonance energy transfer (FRET).

3.3. Antibacterial activity

The antibacterial activity of the benzothiazolyl-pyridinecarbonitrile derivatives were examined against three representative bacterial strains: *Escherichia coli* (ATCC 25922), *Salmonella enterica* (ATCC 14028), and *Staphylococcus aureus* (ATCC 25923). These strains were chosen to assess efficacy against both Gram-negative and Gram-positive bacteria. The compounds were tested at concentrations of 25 μg mL^{-1} and 50 μg mL^{-1} under both dark and light conditions to assess the impact of photoactivation on antibacterial efficacy. Under dark conditions, all four derivatives exhibited no antibacterial activity at both tested concentrations across all three bacterial strains. The minimal zones of inhibition observed in the dark suggest that the compounds are largely inert without light activation, which is a favorable feature for reducing off-target effects during non-irradiated states. However, upon exposure

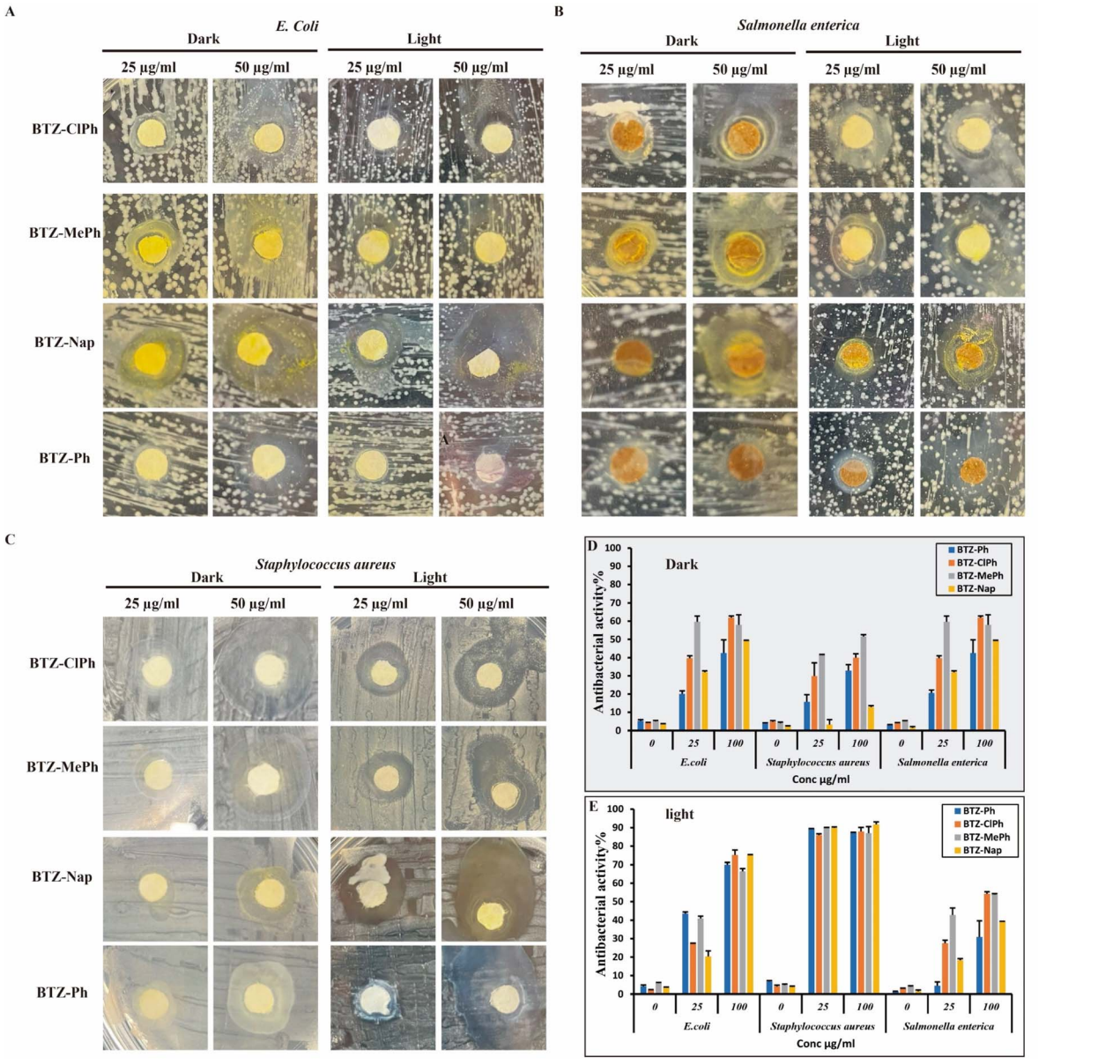

Fig. 6 Antibacterial activity of four benzothiazolyl-pyridinecarbonitrile derivatives—**BTZ-ClPh**, **BTZ-MePh**, **BTZ-Nap**, and **BTZ-Ph**, against *Escherichia coli*, *Salmonella enterica*, and *Staphylococcus aureus* under dark and light exposure. (A) Representative images showing the antibacterial activity against *E. coli* at 25 and 50 μg mL^{-1} concentrations under dark and light conditions. (B) Antibacterial activity against *Salmonella enterica* under the same treatment conditions. (C) Antibacterial activity against *Staphylococcus aureus* at 25 and 50 μg mL^{-1} under dark and light exposure. (D) MIC (% inhibition) at 25 and 100 μg mL^{-1} against all tested strains under dark and light conditions. (E) MIC (% inhibition) at 25 and 100 μg mL^{-1} under light conditions. Zones of inhibition were visually assessed, and antibacterial activity was calculated based on the area of bacterial clearance. Data are shown as mean ± SD from three independent experiments.

to light, a clear enhancement in antibacterial activity was observed, indicating the photosensitive nature of these molecules and their potential role as photoactivated antimicrobial agents. Among the derivatives, **BTZ-Nap** showed the most pronounced antibacterial activity under light conditions. At a concentration of 50 μg mL^{-1}, **BTZ-Nap** generated substantial inhibition zones against *E. coli*, *Salmonella enterica*, and *Staphylococcus aureus*, highlighting its broad-spectrum efficacy. The enhanced activity of **BTZ-Nap** likely arises from its high ability to generate singlet oxygen (as we will discuss in Section 3.6) that damage bacterial cells. Its planar structure also facilitates membrane binding, positioning ROS close to microbes and amplifying oxidative damage for effective antimicrobial action in PDT.[67,68] Similarly, **BTZ-MePh** showed strong light-activated antibacterial activity, particularly against *S. aureus*, indicating that the electron-donating methyl group enhances energy transfer to oxygen, and ROS generation. Methyl substitution also improves photostability and membrane affinity, promoting cellular uptake and accumulation, thereby strengthening overall antimicrobial efficacy.[69] The quantitative data from Fig. 6 further supports these findings. The antibacterial activity of the compounds increased significantly under light, with **BTZ-Nap** achieving more than 80% inhibition in some cases, particularly against *S. aureus* and *Salmonella enterica*. In contrast, **BTZ-Ph** and **BTZ-ClPh** exhibited only moderate enhancement in antibacterial activity upon light exposure, indicating that both the presence and nature of the substituent groups play a critical role in determining photodynamic antibacterial efficacy.

Interestingly, *Staphylococcus aureus*, a Gram-positive organism, appeared more susceptible to the compounds than the Gram-negative strains. This difference in susceptibility may

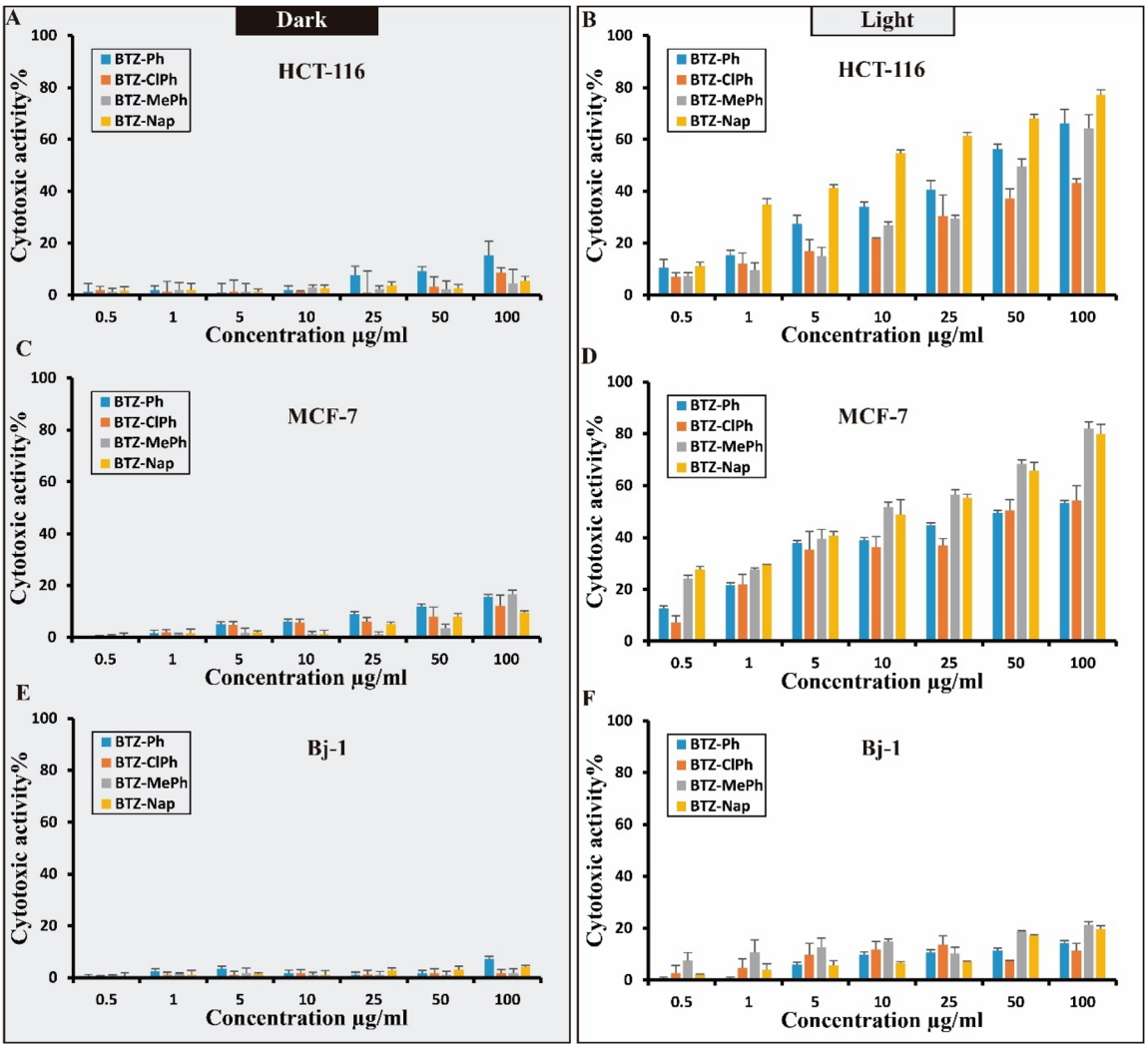

Fig. 7 Cytotoxic activity of benzothiazolyl-pyridinecarbonitrile derivatives (**BTZ-Ph**, **BTZ-ClPh**, **BTZ-MePh**, and **BTZ-Nap**) against HCT-116, MCF-7, and BJ-1 cell lines under dark and light conditions. Cells were treated with increasing concentrations (0.5, 1, 5, 10, 25, 50, and 100 μg mL^{-1}) of each compound. Cytotoxicity was evaluated using a standard viability assay after 24 hours of treatment. (A, C, E) Cytotoxicity under dark conditions for HCT-116 (A), MCF-7 (C), and BJ-1 (E). (B, D, F) Cytotoxicity under light exposure for HCT-116 (B), MCF-7 (D), and BJ-1 (F). Data are presented as mean ± standard deviation (SD) of three independent experiments.

be attributed to the structural differences in bacterial cell walls; the thick but porous peptidoglycan layer in *S. aureus* may allow better diffusion or interaction with the compounds compared to the outer membrane of Gram-negative bacteria, which can act as a permeability barrier. These results clearly demonstrate that the synthesized benzothiazolyl-pyridinecarbonitrile derivatives possess light-dependent antibacterial activity, with **BTZ-Nap** and **BTZ-MePh** being the most effective candidates. Their enhanced activity under light exposure, combined with low dark toxicity, underscores their potential as promising agents for photodynamic antimicrobial applications.

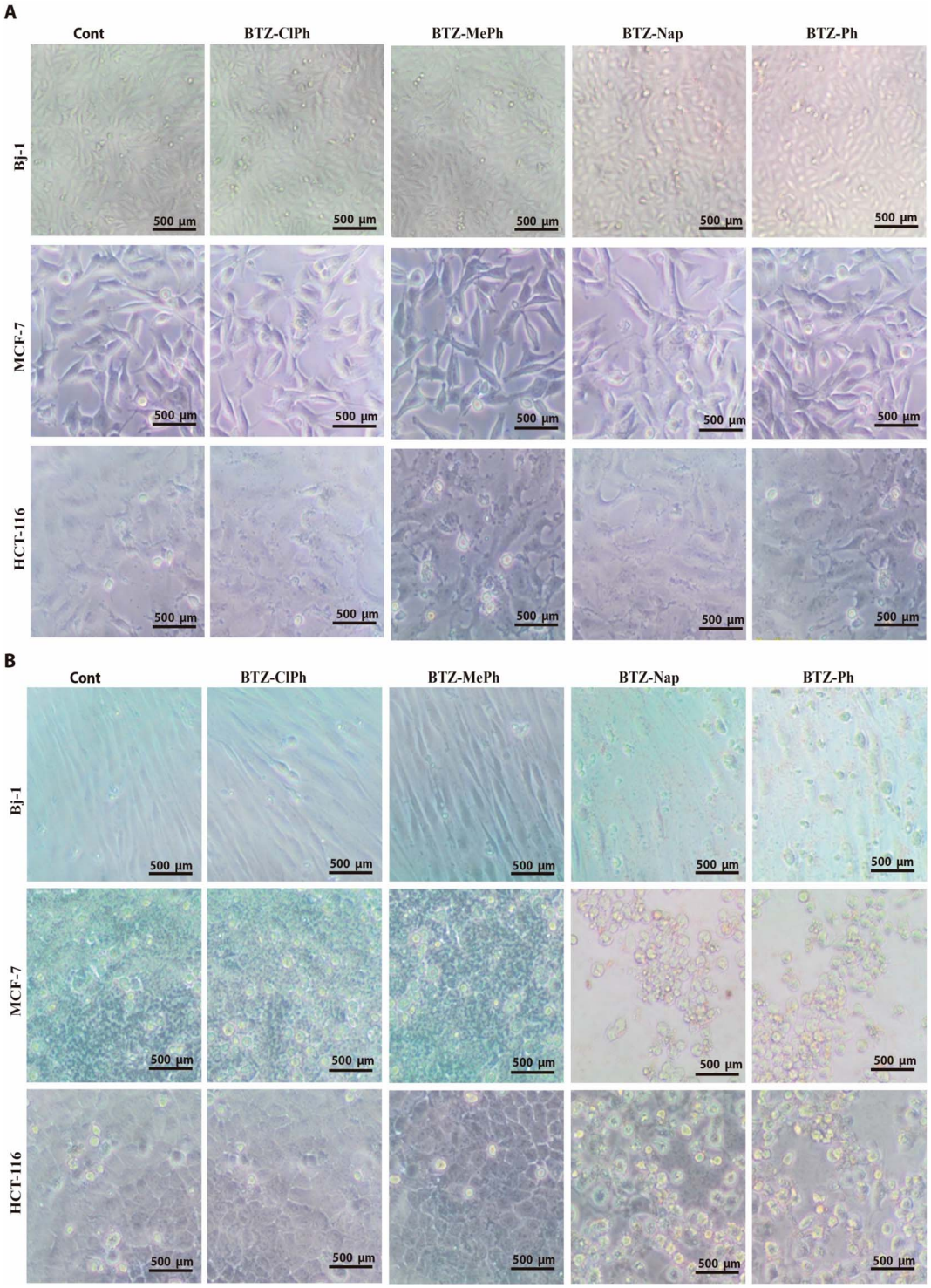

Fig. 8 Microscopic imaging of the cytotoxic activity of benzothiazolyl-pyridinecarbonitrile derivatives (**BTZ-Ph**, **BTZ-ClPh**, **BTZ-MePh**, and **BTZ-Nap**) against HCT-116, MCF-7, and BJ-1 cell lines under light (A) and dark (B) conditions.

3.4. Cytotoxic activity

The cytotoxic effects of the benzothiazolyl-pyridinecarbonitrile derivatives were evaluated against MCF-7 (breast adenocarcinoma), HCT-116 (colorectal carcinoma), and BJ-1 (normal fibroblasts) using the MTT assay under both dark and light irradiation conditions (Fig. 7 A–H). A range of concentrations (0.5–100 μg mL^{-1}) was tested to assess dose-dependent effects.

In the absence of light, all four derivatives exhibited negligible cytotoxicity toward both cancer and normal cell lines. IC_{50} values exceeded 500 μg mL^{-1} in MCF-7 (535.87, 527.76, 519.09, and 639.65 μg mL^{-1} for **BTZ-Ph**, **BTZ-ClPh**, **BTZ-MePh**, and **BTZ-Nap**, respectively) and 700 μg mL^{-1} in HCT-116 (698.23, 732.12, 964.87, and 1104.76 μg mL^{-1} for the respective compounds). This minimal dark toxicity is advantageous for phototherapeutic applications, as it suggests low systemic risk in the absence of photoactivation.

Upon light activation, a marked increase in cytotoxicity was observed in both cancer cell lines. In MCF-7 cells, IC_{50} values decreased dramatically to 69.54, 49.78, 9.86, and 16.54 μg mL^{-1} for **BTZ-Ph**, **BTZ-ClPh**, **BTZ-MePh**, and **BTZ-Nap**, respectively. In HCT-116 cells, corresponding IC_{50} values were 47.65, 147.98, 56.98, and 22.32 μg mL^{-1}. Among the derivatives, **BTZ-Nap** displayed the strongest activity, inducing >85% cell death at 100 μg mL^{-1} in both cancer lines. Its higher efficacy is also related to its high singlet oxygen quantum yield that we will discuss in Section 3.6, which helps anticancer photodynamic treatment (PDT) work better by increasing the number of cancer cells that are selectively destroyed when exposed to light.[70] Both **BTZ-MePh** and **BTZ-ClPh** demonstrated significant levels of phototoxicity; however, **BTZ-MePh** was slightly more active because of its methyl groups, which improved electron density, and photostability, resulting in increased oxidative damage and ROS generation. Additionally, alkylation improves lipophilicity, which enhances cancer cell uptake and accumulation.[71] In contrast, **BTZ-Ph** exhibited only moderate activity, highlighting the influence of aryl substitution on photodynamic efficiency.

Microscopic analysis further supported these findings (Fig. 8). In normal BJ-1 fibroblasts, **BTZ-ClPh** and **BTZ-MePh** preserved healthy morphology, while **BTZ-Nap** and **BTZ-Ph** induced only a mild reduction in cell density, consistent with limited toxicity. In contrast, MCF-7 and HCT-116 cells displayed pronounced cytotoxic responses following light activation, including reduced cell density, rounding, and membrane rupture—hallmarks of apoptotic and/or necrotic cell death. Notably, cytotoxicity in BJ-1 cells remained below 30% across all concentrations and derivatives, indicating preferential activity toward malignant cells.

HCT-116 cells appeared slightly more sensitive to the derivatives than MCF-7, potentially reflecting differences in cellular uptake, metabolic activity, or intrinsic vulnerability to oxidative stress. Overall, the benzothiazolyl-pyridinecarbonitrile derivatives exhibited strong light-dependent anticancer activity, with **BTZ-Nap** emerging as the most potent and selective. The combination of minimal dark toxicity and pronounced photoactivated cytotoxicity underscores their promise as candidates for further development in photodynamic cancer therapy.

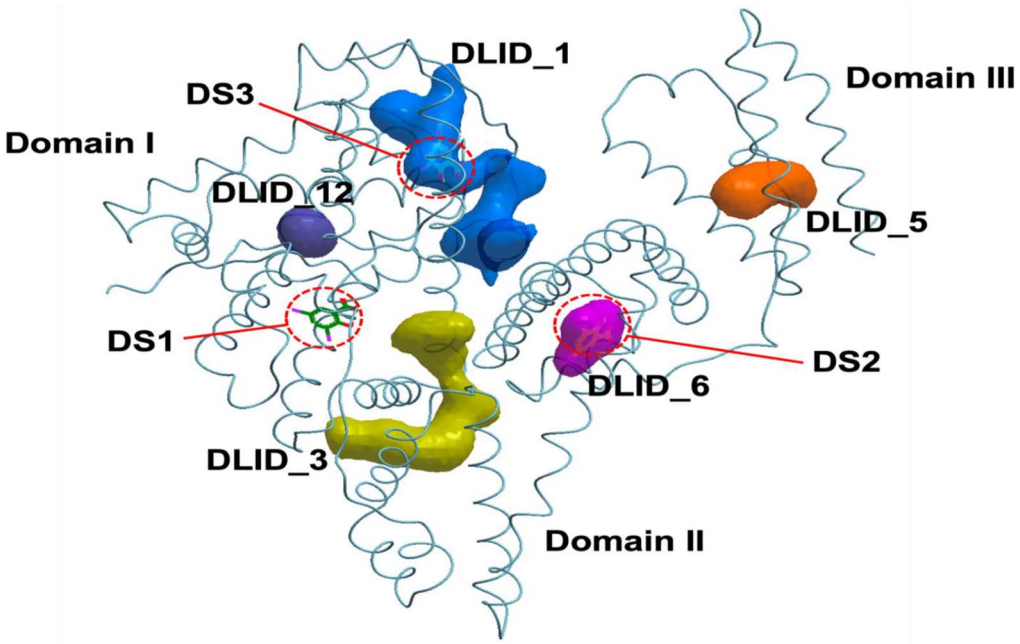

Fig. 9 Potential ligand binding sites on Bovine Serum Albumin (BSA). The figure shows the locations of known drug binding sites (**DS1**, **DS2**, and **DS3**) and predicted druggable pockets (**DLID_1**, **DLID_3**, **DLID_5**, **DLID_6**, and **DLID_12**) on the BSA structure (PDB ID: 4jk4). The known sites are based on the co-crystallized ligand, 3,5-diiodosalicylic acid (green stick models), while the predicted pockets are shown as colored surfaces. Notably, **DS2** overlaps with the **DLID_6** pocket (magenta), and **DS3** overlaps with the **DLID_1** pocket (blue). All sites are distributed across domains I, II, and III of the protein.

3.5. Molecular docking studies

Molecular docking studies were conducted to better understand the structural basis for the binding of the synthesized compounds to BSA. The simulations identified two overlapping high-affinity regions on BSA emerged from docking—**DS3** (overlapping with **DLID_1**) and the adjacent **DLID_1** cavity. **BTZ-ClPh** is anchored in **DS3** by a specific H-bond from its pyridone oxygen to Arg458, whereas **BTZ-Ph** attains high predicted affinity in **DLID_1** *via* π–π stacking with His145 and a putative H-bond to the Tyr147 main-chain amide (Fig. 9, 10 and 11) (Table S1). Our analysis focused on comparing the binding modes of the experimentally most active ligand, **BTZ-ClPh**, and the computationally highest-scoring ligand, **BTZ-Ph**. As illustrated in (Fig. 10), the binding of **BTZ-ClPh** in the **DS3** pocket is primarily anchored by a strong and specific hydrogen bond formed between its pyridone oxygen and the side chain of Arg458. This specific interaction, complemented by numerous hydrophobic contacts, provides a clear structural basis for its high experimental affinity. In contrast, **BTZ-Ph**, which achieved the best docking score of −28.51 in the adjacent **DLID_1** pocket, displays a different binding mode (Fig. 11). It lacks the direct hydrogen bond to Arg458. Instead, its high predicted affinity appears to be derived from a combination of other interactions: a significant π–π stacking interaction with the imidazole ring of His145, and a potential hydrogen bond between its nitrile group and the main-chain amide of Tyr147. This comparative analysis offers a potential explanation for the discrepancy between the experimental affinity order (**BTZ-ClPh** > **BTZ-MePh** > **BTZ-Ph** > **BTZ-Nap**) and the calculated scores.

The higher docking score of **BTZ-Ph** likely reflects predicted hydrogen-bonding in a static pose, whereas experimental results show stronger binding for **BTZ-ClPh**. This discrepancy highlights the greater impact of cumulative noncovalent forces in the dynamic protein environment. The chlorine substituent enhances polarizability, hydrophobic contacts, and potential halogen bonding, collectively stabilizing the complex more effectively than isolated hydrogen bonds, which docking may overemphasize. The docking study, therefore, not only identifies the key binding region on BSA but also elucidates the nuanced differences in molecular interactions that likely govern the compounds' observed activities.

3.6. Singlet oxygen quantum yields for photodynamic therapy

The singlet oxygen quantum yield (Φ_Δ) serves as a key indicator of a material's effectiveness as a photosensitizer in photodynamic therapy (PDT) for cancer treatment. Singlet oxygen ($^1O_2$) is generated through a photosensitized process that requires

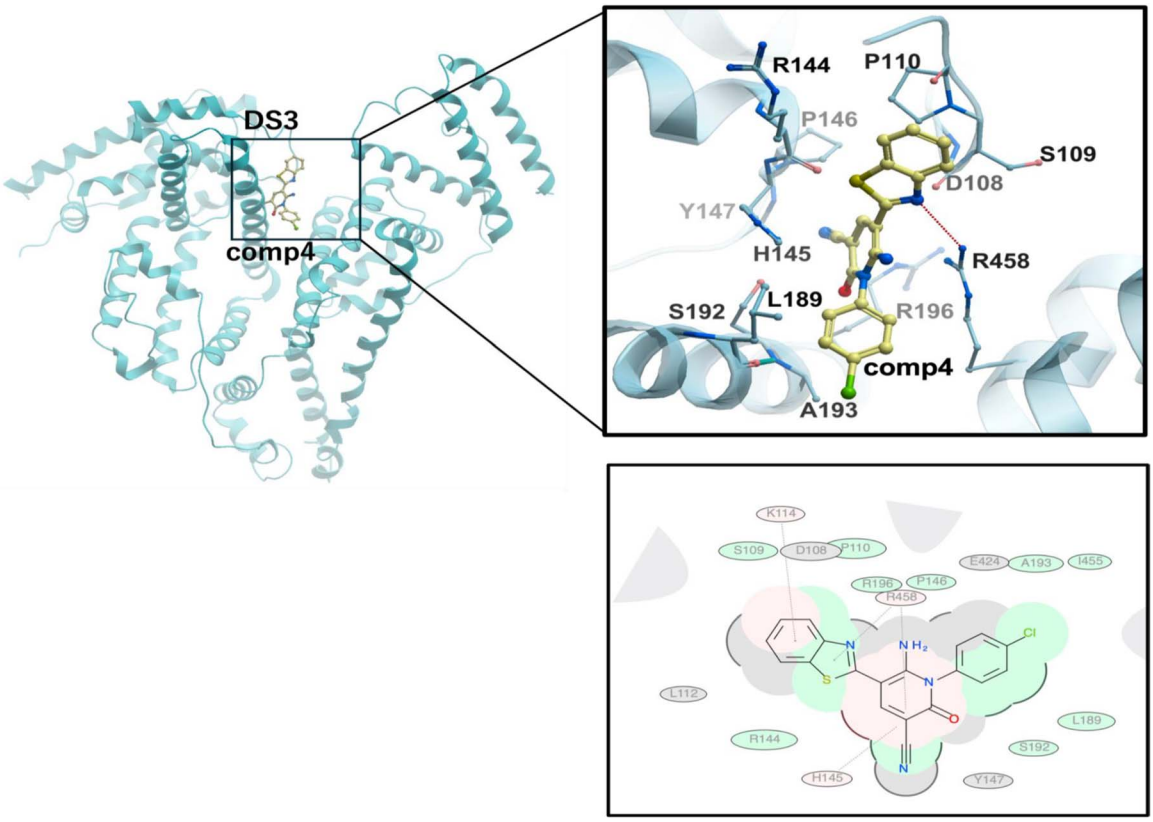

Fig. 10 The predicted binding mode of **BTZ-ClPh** within Drug Site 3 (**DS3**) of BSA. This figure shows the predicted binding of **BTZ-ClPh**, the most active compound, in Drug Site 3 (**DS3**) of the BSA protein. The top-left panel gives an overview, while the top-right and bottom panels detail the interactions. **BTZ-ClPh** (yellow) forms a key hydrogen bond with Arg458 and is stabilized by hydrophobic and van der Waals interactions with residues like Pro110, Pro146, Leu189, and Ala193. The benzothiazole group is also positioned for potential π-stacking with His145 and Tyr147.

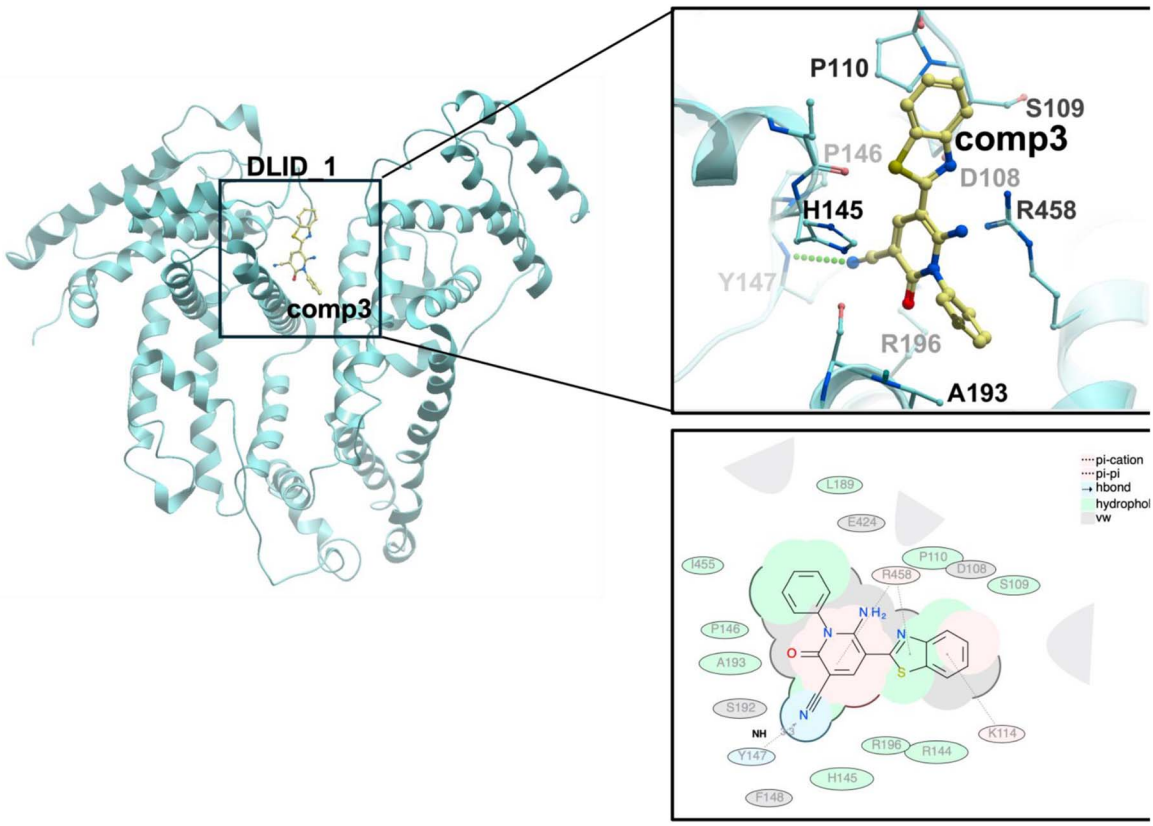

Fig. 11 Shows the predicted binding mode of **BTZ-Ph** in the BSA **DLID_1** pocket, with an optimal docking score of −28.51. The figure provides an overview (top left), a detailed 3D view of interactions (top right), and a 2D schematic (bottom). The high binding affinity is driven by a strong π−π stacking interaction between the benzothiazole ring and the His145 imidazole side chain, and a hydrogen bond between the nitrile group's nitrogen and the main-chain amide of Tyr147. These are supported by a network of hydrophobic and van der Waals contacts with residues like Pro110, Pro146, Ala193, and Arg196.

oxygen, light of an appropriate wavelength, and a photosensitizer to absorb that light.[72,73] Upon photoexcitation, the photosensitizer is first elevated to its singlet excited state, which then undergoes intersystem crossing (ISC) to its longer-lived triplet excited state (T_1), typically on the microsecond timescale. Singlet oxygen is subsequently generated *via* energy transfer from this excited triplet state ($^3P^*$) of the photosensitizer to ground-state triplet oxygen ($^3O_2$) (Fig. 12). The produced singlet oxygen quantum yield (Φ_Δ) is quantified by directly measuring the weak singlet oxygen phosphorescence signal in the near-infrared (NIR) region at approximately 1275 nm in acetonitrile, following a modified McKenzie *et al.* method.[74–77] In this study, Φ_Δ values were obtained under low-energy conditions where singlet oxygen emission decay exhibited a mono-exponential pattern. The kinetic trace obtained was analyzed by a monoexponentially decay using OriginPro ExpDecay1 fitting function (eqn (7)):

$$y = A_1 e^{-(-x-x_0)/t_1} \quad (7)$$

The quantum yield of singlet oxygen generation (Φ_Δ) for the compounds was determined by comparing their extrapolated emission intensity at time zero with that of the standard, $[Ru(bpy)_3]Cl_2$. This standard has a reported singlet oxygen quantum yield of Φ_Δ = 57% in acetonitrile.[78–81] The photosensitized singlet oxygen quantum yields of the examined materials were found to be: **BTZ-Ph** (0.20), **BTZ-ClPh** (0.21), **BTZ-MePh** (0.18), and **BTZ-Nap** (0.31). These values were in good agreement with those reported in the literature for similar compounds.[33] The high Φ_Δ value of **BTZ-Nap** is attributed to the existence of a naphthyl group, which encourages intersystem crossing to the triplet state and stabilizes relevant excited states, leading to higher singlet oxygen quantum yields and improved photosensitizer performance in biomedical and PDT applications.[82]

4. Conclusion

In summary, the interactions between bovine serum albumin (BSA) and four benzothiazolyl-pyridinecarbonitrile derivatives—1-**BTZ-Ph**, 2-**BTZ-ClPh**, 3-**BTZ-MePh**, and 4-**BTZ-Nap** have been well characterized using a multi-spectroscopic approach. The results showed a considerable quenching and lifetime reduction of BSA fluorescence emission upon the addition of BTZ derivatives, and strong spectral overlap between the BSA

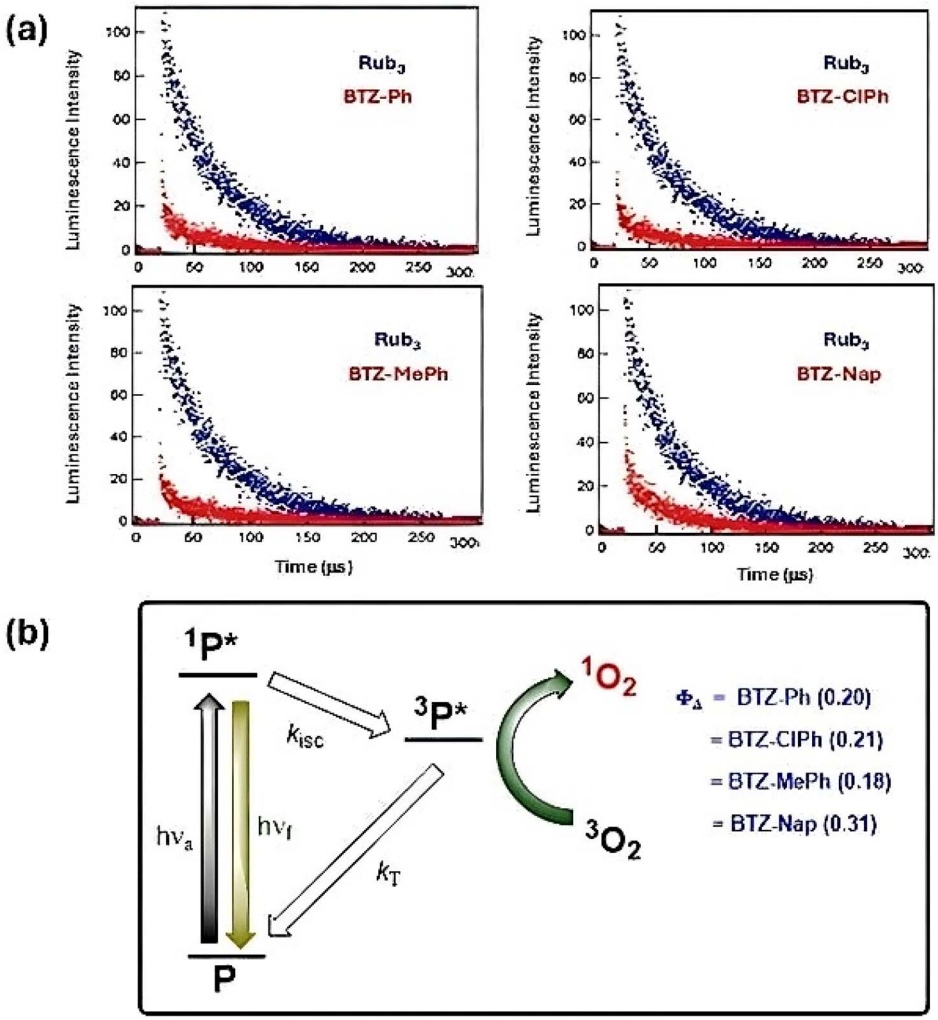

Fig. 12 (a) Decay traces of singlet oxygen phosphorescence at 1275 nm produced by the examined compoundsin acetonitrile; $\lambda_{ex} = 355$ nm. (b) Scheme illustrates the excitation, fluorescence, and singlet oxygen generation (Φ_Δ) pathways of the examined photosensitisers in acetonitrile. $Rub_3 = [Ru(bpy)_3]Cl_2$.

emission spectrum and the absorption spectra of the N-substituted 2-pyridylbenzothiazole derivatives, suggesting that the interaction occurs through dynamic quenching mechanism and energy transfer process (FRET). Importantly, all derivatives exhibited relatively moderate singlet oxygen ($^1O_2$) quantum yields (Φ_Δ); **BTZ-Ph** (0.20), **BTZ-ClPh** (0.21), **BTZ-MePh** (0.18), and **BTZ-Nap** (0.31), rendering them as good photosensitizers for photodynamic therapy applications. Upon blue light irradiation, the compounds exhibited pronounced antibacterial effects against *Salmonella enterica*, *Staphylococcus aureus*, and *E. coli*. Likewise, under the same light conditions, they showed strong cytotoxic activity toward human breast cancer (MCF-7) and colorectal carcinoma (HCT-116) cell lines, while exhibiting minimal toxicity toward normal skin fibroblast cells (Bj-1). Collectively, these findings highlight the potential of these benzothiazole derivatives as promising candidates for both photodynamic therapy (PDT), antimicrobial, and anticancer photodynamic inactivation, warranting further investigation into their *in vivo* efficacy and therapeutic applications.

Conflicts of interest

The authors declare that they have no known competing financial interests or personal relationships that could have appeared to influence the work reported in this paper.

Data availability

Data will be made available on request.

Supplementary information is available. See DOI: **https://doi.org/10.1039/d5ra06375b**.

Acknowledgements

This work supported from the Science, Technology & Innovation Funding Authority (STDF) under grant number 46207. M. E. El-Khouly Acknowledges Prof. Galal H. Elgemeie for providing the examined samples. Hanan Ali gratefully acknowledges the financial support provided by the Egyptian Ministry of Higher

Education (MoHE) scholarship at Egypt-Japan University of Science and Technology (EJUST), which also supported the research by providing the facilities and labs required to conduct this study.

References

1 K. P. Yadav, M. A. Rahman, S. Nishad, S. K. Maurya, M. Anas and M. Mujahid, Synthesis and Biological Activities of Benzothiazole Derivatives: A review, *Intell. Pharm.*, 2023, **1**, 122–132.

2 B. C. Yallur, U. Katrahalli, P. M. Krishna and M. D. Hadagali, BSA binding and antibacterial studies of newly synthesized 5, 6-Dihydroimidazo [2, 1-b] thiazole-2-carbaldehyde, *Spectrochim. Acta, Part A*, 2019, **222**, 117192.

3 N. H. Metwally, G. H. Elgemeie and F. G. Fahmy, Synthesis and biological evaluation of benzothiazolyl-pyridine hybrids as new antiviral agents against H5N1 bird flu and SARS-COV-2 viruses, *ACS Omega*, 2023, **8**, 36636–36654.

4 G. Sharma and R. Sharma, Novel spiro [indoline-3, 2′ thiazolo [5, 4-*e*] pyrimido [1, 2-*a*] pyrimidine] derivatives as possible anti-dermatophytic and anti-candidiasis agent, *Biomed. Khim.*, 2024, **70**(3), 180–186.

5 A. Drakontaeidi, I. Papanotas and E. Pontiki, Multitarget Pharmacology of Sulfur–Nitrogen Heterocycles: Anticancer and Antioxidant Perspectives, *Antioxidants*, 2024, **13**, 898.

6 A. A. Al-Mutairi, H. N. Hafez, A. R. B. El-Gazzar and M. Y. Mohamed, Synthesis and antimicrobial, anticancer and anti-oxidant activities of novel 2, 3-dihydropyrido [2,3-*d*] pyrimidine-4-one and pyrrolo [2,1-*b*][1, 3] benzothiazole derivatives *via* microwave-assisted synthesis, *Molecules*, 2022, **27**, 1246.

7 L. M. Aroua, F. M. Alminderej, H. R. Almuhaylan, A. H. Alosaimi, F. Medini, H. A. Mohammed and N. H. Mekni, Benzimidazole(s): synthons, bioactive lead structures, total synthesis, and the profiling of major bioactive categories, *RSC Adv.*, 2025, **15**, 7571–7608.

8 R. Bora, D. P. Kemisetti, F. Alam, A. Ghosh, A. Dutta, S. Roy and M. I. Judder, Synthesis, *in silico* and Pharmacological Activity of 1, 3-Benzothiazol Derivatives, *J. Young Pharm.*, 2025, **17**, 138–148.

9 M. S. Vasava, M. N. Bhoi, S. K. Rathwa, D. J. Jethava, P. T. Acharya, D. B. Patel and H. D. Patel, Benzimidazole: a milestone in the field of medicinal chemistry, *Mini-Rev. Med. Chem.*, 2020, **20**, 532–565.

10 J. B. Shaik, M. K. M. Pinjari, D. A. Gangaiah and C. G. R. Nallagondu, Synthetic strategies of functionalized pyridines and their therapeutic potential as multifunctional anti-Alzheimer's agents, in *Recent Developments in the Synthesis and Applications of Pyridines*, Elsevier, 2023, pp. 69–126.

11 S. Jaiswal and N. K. Verma, Benzothiazole moiety with sulphonamide as anti-inflammatory and analgesic activity: a review, *South Asian Res. J. Pharm. Sci.*, 2021, **3**, 90–1012.

12 R. C. Duarte, R. Cercená, B. B. de Araujo, O. A. Chaves, P. F. Gonçalves, E. Zapp, F. S. Santos, F. S. Rodembusch and A. G. DaI-Bó, Synthesis, Characterization, and BSA Binding Properties of Carboxylated Merocyanine-Based Fluorophores, *ACS Omega*, 2024, **9**(49), 48697–48710.

13 T. Ghosh and K. Bhadra, A mini review on human serum albumin-natural alkaloids interaction and its role as drug carrier, *J. Biomol. Struct. Dyn.*, 2024, 1–18.

14 O. Adamczyk, M. Szota, K. Rakowski, M. Prochownik, D. Doveiko, Y. Chen and B. Jachimska, Bovine serum albumin as a platform for designing biologically active nanocarriers—experimental and computational studies, *Int. J. Mol. Sci.*, 2023, **25**, 37.

15 S. Tayyab and S. R. Feroz, Serum albumin: clinical significance of drug binding and development as drug delivery vehicle, *Adv. Protein Chem. Struct. Biol.*, 2021, **123**, 193–218.

16 S. Behera, P. Mohanty, P. P. Dash, P. Mohapatra, L. Shubhadarshinee, R. Behura, A. K. Barick, P. Mohapatra and B. R. Jali, Selective binding of bovine serum albumin (BSA): a Comprehensive Review, *Biointerface Res. Appl. Chem.*, 2023, **13**, 555.

17 S. Sengottiyan, K. Malakar, A. Kathiravan, M. Velusamy, A. Mikolajczyk and T. Puzyn, Integrated approach to interaction studies of pyrene derivatives with bovine serum albumin: insights from theory and experiment, *J. Phys. Chem. B*, 2022, **126**, 3831–3843.

18 A. R. Pathania, Chemistry behind serum albumin: a review, in *E3S Web Conf.*, 2021, vol. 309, p. 01086.

19 Z. Y. Hu, W. J. Wang, L. Hu, J. H. Shi and S. L. Jiang, Comprehending the intermolecular interaction of dacomitinib with bovine serum albumin: experimental and theoretical approaches, *J. Biomol. Struct. Dyn.*, 2024, **42**, 3579–3592.

20 B. Mandal, N. Chowdhury, N. Baildya, R. P. Mandal, A. Bagchi and S. De, Fluorescence probing and molecular docking analysis of the binding interaction of bovine serum albumin (BSA) with the polarity probe AICCN, *Phys. Chem. Chem. Phys.*, 2023, **25**, 18197–18214.

21 V. Patil, S. Labade, C. Khilare and S. Sawant, A molecular bridge-like binding mode of buspirone to BSA: multispectroscopic and molecular docking investigation, *Chem. Data Collect.*, 2022, **40**, 100892.

22 S. Behera, R. Behura, P. Mohanty, M. Sahoo and R. Duggirala, Study of interaction between bovine serum albumin and dolutegravir intermediate: fluorescence and molecular docking analysis, *Biointerface Res. Appl. Chem.*, 2021, **11**, 13102–13110.

23 C. Erkmen and M. Z. Kabir, Current analytical methods and applications used in the insight of serum proteins interactions with various food additives, pesticides, and contaminants, *Explor. Foods Foodomics*, 2024, **2**, 195–222.

24 L. Wang, W. Zhang, Y. Shao, D. Zhang, G. Guo and X. Wang, Analytical methods for obtaining binding parameters of drug–protein interactions: a review, *Anal. Chim. Acta*, 2022, **1219**, 340012.

25 U. Katrahalli, G. Shanker, D. Pal and M. D. Hadagali, Molecular spectroscopic and docking analysis of the interaction of fluorescent thiadicarbocyanine dye with

biomolecule bovine serum albumin, *J. Biomol. Struct. Dyn.*, 2023, **41**, 10702–10712.

26 M. L. Kabir, F. Wang and A. H. Clayton, Intrinsically fluorescent anti-cancer drugs, *Biology*, 2022, **11**, 1135.

27 A. Saini and P. Bansal, Quenching studies as important toolkit for exploring binding propensity of metal complexes with serum albumin and DNA (a review), *Pharm. Chem. J.*, 2022, **56**(4), 545–558.

28 E. Serag, E. M. El-Fakharany, S. F. Hammad and M. E. El-Khouly, Metal-organic frawork MIL-101(Fe) functionalized with folic acid as a multifunctional nanocarrier for targeted chemotherapy-photodynamic therapy, *Biomater. Sci.*, 2025, **13**, 2351.

29 Y. Yue, B. Li, D. Wang, C. Wu, Z. Li and B. Liu, Optimizing Photosensitizers with Type I and Type II ROS Generation Through Modulating Triplet Lifetime and Intersystem Crossing Efficiency, *Adv. Funct. Mater.*, 2025, **35**, 2414542.

30 N. Singh, R. S. Gupta and S. Bose, A comprehensive review on singlet oxygen generation in nanomaterials and conjugated polymers for photodynamic therapy in the treatment of cancer, *Nanoscale*, 2024, **16**, 3243–3268.

31 P. S. Maharjan and H. K. Bhattarai, Singlet oxygen, photodynamic therapy, and mechanisms of cancer cell death, *J. Oncol.*, 2022, **2022**, 7211485.

32 R. R. Cheruku, J. Cacaccio, F. Durrani, W. A. Tabaczynski, R. Watson, A. J. Marko, R. Kumar, M. E. El-Khouly, S. Fukuzumi, J. R. Missert, R. Yao, M. Sajjad, D. Chandra, K. Guru and R. K. Pandey, Epidermal Growth Factor Receptor-Targeted Multifunctional Photosensitizers for Bladder Cancer Imaging and Photodynamic Therapy, *J. Med. Chem.*, 2019, **62**(5), 2598–2617.

33 S. K. Seth, C. Acquah, L. Levi, S. Jockusch and C. E. Crespo-Hernández, Harnessing the Excited States of 5-(5-Phenylthiophen-2-yl)-6-Azauridine as a Three-Pronged Agent for Skin Cancer Therapy: Photodynamic Action, Cell Imaging, and Cancer Cell Inhibition, *ACS Appl. Bio Mater.*, 2025, **8**(8), 7357–7369.

34 C. Wince, C. T. Kassa, J. Insper, D. Amzallag, W. Consonlandich, A. C. A. Tortamano and R. A. Prates, Antimicrobial photodynamic therapy effects mediated by methylene blue in surfactant medium as an adjuvant treatment of teeth with apical periodontitis and presence of fistula–Protocol for randomized, controlled, double-blind clinical trial, *PLoS One*, 2024, **19**(12), e0315169.

35 S. Verma, U. W. Sallum, H. Athar, L. Rosenblum, J. W. Foley and T. Hasan, Antimicrobial photodynamic efficacy of side-chain functionalized benzo [a] phenothiazinium dyes, *Photochem. Photobiol.*, 2009, **85**(1), 111–118.

36 L. A. Ortiz-Rodríguez, Y. G. Fang, G. Niogret, K. Hadidi, S. J. Hoehn, H. J. Folkwein and C. E. Crespo-Hernández, Thieno [3, 4-d] pyrimidin-4 (3 H)-thione: an effective, oxygenation independent, heavy-atom-free photosensitizer for cancer cells, *Chem. Sci.*, 2023, **14**(33), 8831–8841.

37 R. A. Azzam, G. H. Elgemeie and R. R. Osman, Synthesis of novel pyrido [2,1-*b*] benzothiazole and N-substituted 2-pyridylbenzothiazole derivatives showing remarkable fluorescence and biological activities, *J. Mol. Struct.*, 2020, **1201**, 127194.

38 K. Mousa, A. Abd El-Moneim, S. F. El-Mashtoly, M. M. Mohamed and M. E. El-Khouly, Laser-induced graphene functionalized cationic porphyrin: fabrication, characterization, and intra-supramolecular electron transfer process, *RSC Adv.*, 2025, **15**, 289–300.

39 A. Ansary, A. Osman and M. E. El-Khouly, Doxorubicin-loaded pH-responsive porphyrin-derived carbon dots as a promising biocompatible drug delivery system for effective chemotherapy of breast cancer, *RSC Adv.*, 2025, **15**, 6457–6473.

40 E. Serag, M. Helal and A. El Nemr, Curcumin loaded onto folic acid carbon dots as a potent drug delivery system for antibacterial and anticancer applications, *J. Cluster Sci.*, 2024, **35**, 519–532.

41 H. N. Akl, D. Salah, H. S. Abdel-Samad, A. A. Abdel Aziz and A. A. Abdel-Shafi, Fractional dependence of the free energy of activation on the driving force of charge transfer in the quenching of the excited states of substituted phenanthroline homoleptic ruthenium (ii) complexes in aqueous medium, *RSC Adv.*, 2023, **13**, 13314–13323.

42 M. Pourhajibagher, L. R. Omrani, M. Noroozian, Z. Ghorbanzadeh and A. Bahador, In vitro antibacterial activity and durability of a nano-curcumin-containing pulp capping agent combined with antimicrobial photodynamic therapy, *Photodiagn. Photodyn. Ther.*, 2021, **33**, 102150.

43 T. M. S. F. de Aguiar Coletti, L. M. De Freitas, A. M. F. Almeida and C. R. Fontana, Optimization of antimicrobial photodynamic therapy in biofilms by inhibiting efflux pump, *Photomed. Laser Surg.*, 2017, **35**, 378–385.

44 T. H. Wang, L. F. Chou, Y. W. Shen, N. C. Lin, Y. H. Shih and T. M. Shieh, Mechanistic insights into temoporfin-based photodynamic therapy: ferroptosis as a critical regulator under normoxic and hypoxic conditions in head and neck cancer, *J. Photochem. Photobiol., B*, 2025, 113165.

45 B. Sekula, M. Bilska, B. Wiatrak and A. Bujacz, The crystal structure of bovine serum albumin in the complex with 3,5-diiodosalicylic acid, *Int. J. Biol. Macromol.*, 2013, **60**, 316–324.

46 R. A. Abagyan, M. M. Totrov and D. N. Kuznetsov, ICM—a new method for protein modeling and design: applications to docking and structure prediction from the distorted native conformation, *J. Comput. Chem.*, 1994, **15**, 488–506.

47 J. An, M. Totrov and R. Abagyan, Pocketome *via* comprehensive identification and classification of ligand binding envelopes, *Mol. Cell. Proteomics*, 2005, **4**, 752–761.

48 G. Bottegoni, I. Kufareva, M. Totrov and R. Abagyan, A new method for ligand docking to flexible receptors by dual alanine scanning and refinement (SCARE), *J. Comput.-Aided Mol. Des.*, 2008, **22**, 311–325.

49 S. C. A. Yeh, M. S. Patterson, J. E. Hayward and Q. Fang, Time-resolved fluorescence in photodynamic therapy, *Photonics*, 2014, **1**, 530–564.

50 S. Y. Bi, D. Q. Song, Y. Tian, X. Zhou, Z. Y. Liu and H. Q. Zhang, Molecular spectroscopic study on the interaction of tetracyclines with serum albumins, *Spectrochim. Acta, Part A*, 2005, **61**, 629–636.

51 X.-W. Li, X.-J. Li, Y.-T. Li, Z.-Y. Wu and C.-W. Yan, Syntheses and structures of new trimetallic complexes bridged by *N*-(5-chloro-2-hydroxyphenyl)-*N*′-[3-(dimethylamino)propyl] oxamide: cytotoxic activities, and reactivities towards DNA and protein, *J. Photochem. Photobiol., B*, 2013, **118**, 22.

52 A. W. Tanveer, H. B. Ahmed, A. A.-M. Abdul-Rahman, A. B. Mashooq and Z. Seema, Study of the interactions of bovine serum albumin with the new anti-inflammatory agent 4-(1,3-Dioxo-1,3-dihydro-2*H*-isoindol-2-yl)-N0-[(4-ethoxy-phenyl) methylidene] benzohydrazide using a multi-spectroscopic approach and molecular docking, *Molecules*, 2017, **22**, 1258.

53 M. L. Verteramo, M. M. Ignjatović, R. Kumar, S. Wernersson, V. Ekberg, J. Wallerstein, G. Carstrom, V. Chadimova, H. Leffler, F. Zetterberg, D. T. Logan, U. Ryde, M. Akke and U. J. Nilsson, Interplay of halogen bonding and solvation in protein–ligand binding, *iScience*, 2024, **4**(19), 109636.

54 C. S. Leung, S. S. Leung, J. Tirado-Rives and W. L. Jorgensen, Methyl effects on protein–ligand binding, *J. Med. Chem.*, 2012, **55**(9), 4489–4500.

55 K. Karami, Z. Mehri Lighvan, H. Farrokhpour, M. Dehdashti Jahromi and A. A. Momtazi-Borojeni, Synthesis and spectroscopic characterization study of new palladium complexes containing bioactive O,O-chelated ligands: evaluation of the DNA/protein BSA interaction, *in vitro* antitumoural activity and molecular docking, *J. Biomol. Struct. Dyn.*, 2018, **36**, 3324.

56 P. Joshi, S. Chakraborty, S. Dey, V. Shanker, Z. A. Ansari and S. P. Singh, Binding of chloroquine–conjugated gold nanoparticles with bovine serum albumin, *J. Colloid Interface Sci.*, 2011, **355**, 402–409.

57 B.-L. Wang, D.-Q. Pan, K.-L. Zhou, Y.-Y. Lou and J.-H. Shi, Multi-spectroscopic approaches and molecular simulation research of the intermolecular interaction between the angiotensin-converting enzyme inhibitor (ACE inhibitor) benazepril and bovine serum albumin (BSA), *Spectrochim. Acta, Part A*, 2019, **212**, 15–24.

58 E. Ramachandran, S. P. Thomas, P. Poornima, P. Kalaivani, R. Prabhakaran, V. V. Padma and K. Natarajan, Evaluation of DNA binding, antioxidant and cytotoxic activity of mononuclear Co(III) complexes of 2-oxo-1,2-dihydrobenzo [h]quinoline-3-carbaldehyde thiosemicarbazones, *Eur. J. Med. Chem.*, 2012, **50**, 405–415.

59 D. S. Raja, N. S. P. Bhuvanesh and K. Natarajan, A novel water soluble ligand bridged cobalt(ii) coordination polymer of 2-oxo-1,2-dihydroquinoline-3-carbaldehyde (isonicotinic) hydrazone: evaluation of the DNA binding, protein interaction, radical scavenging and anticancer activity, *Dalton Trans.*, 2012, **41**, 4365–4377.

60 D. S. Raja, E. Ramachandran, N. S. P. Bhuvanesh and K. Natarajan, Synthesis, structure and *in vitro* pharmacological evaluation of a novel 2-oxo-1, 2-dihydroquinoline-3-carbaldehyde (2′-methylbenzoyl) hydrazine bridged copper (II) coordination polymer, *Eur. J. Med. Chem.*, 2013, **64**, 148–159.

61 J. N. Miller, Recent advances in molecular luminescence analysis, *Proc. Anal. Div. Chem. Soc.*, 1979, **16**, 203–208.

62 P. Sathyadevi, P. Krishnamoorthy, N. S. P. Bhuvanesh, P. Kalaiselvi, V. V. Padma and N. Dharmaraj, Organometallic ruthenium(II) complexes: synthesis, structure and influence of substitution at azomethine carbon towards DNA/BSA binding, radical scavenging and cytotoxicity, *Eur. J. Med. Chem.*, 2012, **55**, 420–431.

63 J. Lakowicz, *Principles of Fluorescence Spectroscopy*, Springer, US, 2006.

64 T. Förster and O. Sinanoglu, *Modern Quantum Chemistry*, Academic Press, New York, 1965, vol. 3, pp. 93–137.

65 U. Kragh-Hansen, Molecular aspects of ligand binding to serum albumin, *Pharmacol. Rev.*, 1981, **33**, 17.

66 P. B. Kandagal, S. Ashoka, J. Seetharamappa, S. M. T. Shaikh, Y. Jadegoud and O. B. Ijare, Study of the interaction of an anticancer drug with human and bovine serum albumin: spectroscopic approach, *J. Pharm. Biomed. Anal.*, 2006, **41**, 393–399.

67 L. He, S. Yang, W. Xuan, X. Zhen, Q. Qi, Y. Qi, Q. Li, m. Du, M. R. Hamblin and L. Huang, Phenylalanine-Arginine-β-Naphthylamide Enhances the Photobactericidal Effect of Methylene Blue on Pseudomonas aeruginosa, Photobiomodulation, *Photomed., Laser Surg.*, 2023, **41**(10), 569–575.

68 D. Staneva, A. I. Said, E. Vasileva-Tonkova and I. Grabchev, Enhanced photodynamic efficacy using 1, 8-naphthalimides: potential application in antibacterial photodynamic therapy, *Molecules*, 2022, **27**(18), 5743.

69 J. Ghorbani, D. Rahban, S. Aghamiri, A. Teymouri and A. Bahador, Photosensitizers in antibacterial photodynamic therapy: an overview, *Laser Therapy*, 2018, **27**(4), 293–302.

70 Y. Yuan, Z. Wang, R. Yang, T. Qian and Q. Zhou, Naphthyl quinoxaline thymidine conjugate is a potent anticancer agent post UVA activation and elicits marked inhibition of tumor growth through vaccination, *Eur. J. Med. Chem.*, 2019, **171**, 255–264.

71 G. Varvuolytė, E. Řezníčková, S. Krikštolė, R. Tamulienė, A. Bieliauskas, L. Malina, V. Vojackava, Z. Duben, H. Kolarova, N. Kleiziene, E. Arbaciauskiene, A. Zukausskaite, V. Krystof, A. Sackus and A. Šačkus, Synthesis and photo-induced anticancer activity of new 2-phenylethenyl-1*H*-benzo [*e*] indole dyes, *Eur. J. Med. Chem.*, 2024, **277**, 116777.

72 S. Cui, X. Guo, S. Wang, Z. Wei, D. Huang, X. Zhang and Z. Huang, Singlet oxygen in photodynamic therapy, *Pharmaceuticals*, 2024, **17**(10), 1274.

73 K. K. H. Wang, J. C. Finlay, T. M. Busch, S. M. Hahn and T. C. Zhu, Explicit dosimetry for photodynamic therapy: macroscopic singlet oxygen modeling, *J. Biophotonics*, 2010, **3**(5-6), 304–318.

74 L. K. McKenzie, I. V. Sazanovich, E. Baggaley, M. Bonneau, V. Guerchals, J. A. G. Williams, J. A. Weinstein and H. E. Baryant, Metal Complexes for Two-Photon

Photodynamic Therapy: A Cyclometallated Iridium Complex Induces Two-Photon Photosensitization of Cancer Cells under Near-IR Light, *Chem.–Eur. J.*, 2017, **23**, 234–238.

75 N. M. Shavaleev, H. Adams, J. Best, R. Edge, S. Navaratnam and J. Weinstein, Deep-red luminescence and efficient singlet oxygen generation by cyclometalated platinum(II) complexes with 8-hydroxyquinolines and quinoline-8-thiol, *Inorg. Chem.*, 2006, **45**, 9410–9415.

76 P. R. Ogilby and C. S. Foote, Chemistry of singlet oxygen, Singlet molecular oxygen luminescence in solution following pulsed laser excitation. Solvent deuterium isotope effects on the lifetime of singlet oxygen, *J. Am. Chem. Soc.*, 1982, **104**, 2069–2070.

77 J. R. Hurst, J. McDonald and G. B. Schuster, Lifetime of singlet oxygen in solution directly determined by laser spectroscopy, *J. Am. Chem. Soc.*, 1982, **104**, 2065–2067.

78 J. Parker and W. Stanbro, Optical determination of the collisional lifetime of singlet molecular oxygen in acetone and deuterated acetone, *J. Am. Chem. Soc.*, 1982, **104**, 2067–2069.

79 A. A. Abdel-Shafi, M. D. Ward and R. Schmidt, Mechanism of quenching by oxygen of the excited states of ruthenium(II) complexes in aqueous media. Solvent isotope effect and photosensitized generation of singlet oxygen, $O_2(^1\Delta_g)$, by $[Ru(diimine)(CN)_4]_2$−complex ions, *Dalton Trans.*, 2007, **24**, 2517–2527.

80 R. Schmidt, C. Taniellian, R. Dunsbach and C. Wolff, Phenalenone, a universal reference compound for the determination of quantum yields of singlet oxygen O_2 $(^1\Delta_g)$ sensitization, *J. Photochem. Photobiol., A*, 1994, **79**, 11–17.

81 A. A. Abdel-Shafi, P. D. Beer, R. J. Mortimer and F. Wilkinson, Photosensitized generation of singlet oxygen from ruthenium (II)-substituted benzoaza-crown-bipyridine complexes, *Phys. Chem. Chem. Phys.*, 2000, **2**, 3137–3144.

82 S. Mishra, S. B. Shelar, S. Rout, P. A. Hassan, K. C. Barick and N. Agarwal, Enhamced singlet oxygen generation in aggregates of naphthalene-fused BODIPY and its application in photodynamic therapy, *ACS Appl. Bio Mater.*, 2024, **11**, 7207–7218.